REPORT DOCUMENTATION PAGE

AFRL-SR-BL-TR-01-

0074

1. AGENCY USE ONLY (Leave blank)	2. REPORT DATE	3. REPORT TYPE AND DATES COVERED
	November 16, 2000	Final Technical (1/1/1998-11/30/2000)

4. TITLE AND SUBTITLE
Investigation of Critical Problems in GaN/AlGaN Modfets

5. FUNDING NUMBERS
Grant #F49620-98-1-0042
PO #FQ8671-0000060

6. AUTHOR(S)
Hadis Morkoç, Ph.D.

7. PERFORMING ORGANIZATION NAME(S) AND ADDRESS(ES)

Virginia Commonwealth University
School of Engineering
PO Box 843068
Richmond, VA 23284-3068

8. PERFORMING ORGANIZATION REPORT NUMBER
Final Technical for #528378

9. SPONSORING / MONITORING AGENCY NAME(S) AND ADDRESS(ES)

AFOSR/NE
801 N. Randolph St., Room 732
Arlington, VA 22203-1977

10. SPONSORING / MONITORING AGENCY REPORT NUMBER

11. SUPPLEMENTARY NOTES

12a. DISTRIBUTION / AVAILABILITY STATEMENT

APPROVED FOR PUBLIC RELEASE,
DISTRIBUTION UNLIMITED

12b. DISTRIBUTION CODE

13. ABSTRACT *(Maximum 200 Words)*

MBE AlN layers have been optimized on sapphire substrates. MBE GaN layers have been optimized with ammonia and RF nitrogen sources and Ga polarity films have been consistently obtained using both ammonia and RF nitrogen. With ammonia grown GaN, excellent X-Ray diffraction (1.6 and 3.2 arcmin FWHM values for [002] and [104] diffraction peaks), and PL with only the exciton peak dominating at 10 K with 95 % radiative efficiency have been in 0. 4 μm thick films. The roughness is under 1 nm. Polarization effects on MODFETs have been theoretically treated by effective mass and tight binding calculations in collaboration with Prof. Aldo DiCarli of Universita` di Roma "Tor Vergata. Defects in GaN as manifested in optical transitions have been analyzed. Photoenhanced Electro Chemical (PEC) etching in conjunction with cross-sectional AFM has been developed to investigate structural defect density and correlate them to MBE growth conditions. Initial development of EFM as pertained to polarization issues in GaN has been initiated.

14. SUBJECT TERMS	15. NUMBER OF PAGES
GaN/AlGaN, Modfets, Substrates, Inhomogeneities	58
	16. PRICE CODE

17. SECURITY CLASSIFICATION OF REPORT	18. SECURITY CLASSIFICATION OF THIS PAGE	19. SECURITY CLASSIFICATION OF ABSTRACT	20. LIMITATION OF ABSTRACT
Unclassified	Unclassified	Unclassified	SAR

20010221142

FINAL REPORT: F49620-98-1-0042, H. Morkoc (1/1/98-11/30/00)

1. MBE AlN layers have been optimized on sapphire substrates: See **appendix A**
2. MBE GaN layers have been optimized with ammonia and RF nitrogen sources and Ga polarity films have been consistently obtained using both ammonia and RF nitrogen. With ammonia grown GaN, excellent X-Ray diffraction (1.6 and 3.2 arcmin FWHM values for [002] and [104] diffraction peaks), and PL with only the exciton peak dominating at 10 K with 95 % radiative efficiency have been in 0. 4 μm thick films. The roughness is under 1 nm. For detailed description of the RF grown GaN layers, refer to **appendix B**
3. Polarization effects on MODFETs have been theoretically treated by effective mass and tight binding calculations in collaboration with Prof. Aldo DiCarli of Universita` di Roma "Tor Vergata". See **Appendix C**. Figures are not included to keep the size of the document smaller. They can be provided upon request.
4. Defects in GaN as manifested in optical transitions have been analyzed. See **Appendix D**.

5. Photoenhanced Electro Chemical (PEC) etching in conjunction with cross-sectional AFM has been developed to investigate structural defect density and correlate them to MBE growth conditions. See **Appendix E**.

6. Initial development of EFM as pertained to polarization issues in GaN has been initiated. See **Appendix F**. Figures are not included to keep the size of the document smaller. They can be provided upon request.

Publications

H. Morkoç, "Nitride Semiconductors and Devices", Springer Verlag 1999. ISSN 0933-033x, ISBN 3-540-64038

Roberto Cingolani, A. Botchkarev, H. Tang , Hadis Morkoç, Giuliano Colií and Mauro Lomascolo, A. Di Carlo, and P.Lugli, "Spontaneous polarization and piezoelectric field in $GaN/Al_{0.15}Ga_{0.85}N$ quantum wells: impact on the optical spectra" Phys. Rev. B, in press.

H. Morkoç, "Wurtzite GaN Based Modulation Doped FETs and UV Detectors" Naval Research Review, Vol. 51, No. 1. pp. 28-45 (1999).

P. Ruterana, B. Barbaray, A. Bere, P. Vermaut, A. Hairie, G. Nouet, A. Salvador, A. Botchkarev, and H. Morkoç, "Formation mechanism and relative stability of the {112bar0} stacking fault atomic configurations in wurtzite (Al,Ga,In) nitrides", Physical Review B-Condensed Matter, vol.59, no.24, 15 June 1999, pp.15917-25.

Hadis Morkoç and Roberto Cingolani, and Bernard Gil, "Polarization Effects in Nitride Semiconductors and Device Structures", Materials Research Innovations, Vol.3, No.2, pp. 97-106, 1999.

Hadis Morkoç and Roberto Cingolani, and Bernard Gil, "Polarization Effects in Nitride Semiconductor Device Structures, and Performance of Modulation Doped Field Effect Transistors" Solid State Electronics, vol.43, no.10, pp.1909-1927,October 1999,.

B. H. Bairamov, Ö. Gürdal, A. Botchkarev and H. Morkoç, G. Irmer and J. Monecke, "Direct experimental evidence of tensile strain in wurtzite strucure n-GaN layers grown on n-Si (111) using AlN buffer",Phy. Rev. B. in press

Pierre Lefebvre, Bernard Gil, Jean Massies, Nicolas Grandjean and Mathieu Leroux, Pierre Bigenwald, and Hadis Morkoç, "All that you ever wanted to know about the current status of the physics of nitride-based quantum wells, superlattices, but never tried to ask", in ..... Edited by Manasreh

Bernard Gil, Pierre Lefebvre and Hadis Morkoç, "Strain effects in GaN epilayers" C.R.Acad.Sci. Paris, t.100, Series IV, pp 51-60, 2000 The Compte Rendu à l'académie des Sciences) Michel Voos - Editor.

A. Bonfiglio, M. Lomascolo, G. P. Traetta, R. Cingolani, F.Della Sala, A. DiCarlo, P. Lugli, A. Botchkarev and H. Morkoç, "Well-width dependence of the ground level emission of GaN/AlGaN quantum wells" J. Appl. Phys. In press.

Tomasz J. Ochalski, Bernard Gil, Pierre Lefebvre, Nicolas Grandjean, Mathieu Leroux, Jean Massies, Shuji Nakamura, and Hadis Morkoç, "Photoreflectance investigation of the band-gap in $Al_xGa_{1-x}N$: Evidence of a quasi-zero bowing parameter" Appl. Phys. Letts. Vol. 74, No. 22, pp. 3353-3355, 1999.

Hadis Morkoç, "Recent Developments in Microelectronics and Optoelectronics: A connector to Bioelectronics?", "Science at the Turn of the Millennium" Stuff for Keinan of Scripps Institute.

Hadis Morkoç, Aldo Di Carlo and R. Cingolani, "GaN-Based Modulation Doped FETs and UV Detectors", Condensed Matter News, Ed. Patrick Bernier, in press.

M.I. Nathan, J.E. Borton, C.Cai, P. Chow, J.M. Van Hove, A.Wowchak, and H. Morkoç, "Bias assisted room temperature photochemical (PEC) etching of GaN" Third International Conference on Nitride Semiconductors, July 5-9, 1999, Montpellier France

Hadis Morkoç, "Wurtzite GaN Based Modulation Doped FETs and UV Detectors" Academic Press, Ed. C.E.C. Wood, in press.

H. Morkoç, "Properties of Nitride Semiconductors," in *"Encyclopedia of Materials*: Science and Technology" Eds. D. Bloor, M. C. Fleming, R. J. Brook, S. Mahajan, Senior Ed. R. W. Cahn, 79-Pergamon Press, in press.

J. E. Brown, C. Cai, M. I. Nathan, P. Chow, J. M. Van Hove, A. Wowchak, and H. Morkoç, " Bias assisted, room temperature photoelectrochemical (PEC) etching of p-type GaN", Appl. Phys. Letts. In press.

Presentations

H. Morkoç, Roberto Cingolani, Walter Lambrecht, Bernard Gil, H.-X Jiang and J. Lin, and D. Pavlidis "Spontaneous polarization and piezoelectric field in Nitride Semiconductor Heterostructures", Proc. of the 9th International Symposium on the Physics of Semiconductors and Applications, Nov. 6-7, 1998, Seoul, Korea. Journal of the Korean Physical Society, Vol. 34, supplementary issue, pp. S224-S233, June 1999.

H. Morkoç, Roberto Cingolani, Walter Lambrecht, Bernard Gil, H.-X Jiang and J. Lin, D. Pavlidis, and K.Shenai "Material Properties of GaN in the Context of Electron Devices" Presented at Fall 1998 Meeting of the Materials Research Society, Nov. 29-Dec. 4, 1998 Boston MA USA, Proc. Of Materials Research Society, "GaN and Related Alloys" Eds. C. R. Abernathy and B. Monemar, Vol. 537, p. G.1.2, and MRS Internet Journal, vol.4S1, 1999 INVITED

H.S. Kim, J.Y. Lin, and H.X. Jiang, W.W. Chow, A. Botchkarev and H. Morkoç, "Piezoelectric Effects in GaN/AlGaN Multiple Quantum Wells Probed by Picosecond Time-Resolved Photoluminescence", Presented at Fall 1998 Meeting of the Materials Research Society, Nov. 29-Dec. 4, 1998 Boston MA USA, Proc. Of Materials Research Society, "GaN and Related Alloys" Eds. C. R. Abernathy and B. Monemar, MRS Internet Journal of Nitride Semiconductor Research, vol.4S1, 1999, Publisher: Mater. Res. Soc, USA.

Fabio Della Sala, Aldo Di Carlo, Paolo Lugli, Roberto Cingolani, G. Coli, M. Lomascolo, A. Botchkarev, H. Tang, and H. Morkoç, "Carrier Screening and Polarization Fields in Nitride Based Heterostructure Devices" in Proc. of Advanced Workshop on 'Frontiers in Electronics' (WOFE) May 31-June 4 (1999) Villard de Lans, France.

H. Morkoç, Roberto Cingolani, F. Della Sala, A. DiCarlo, P. Lugli, and B. Gil "Polarization Issues in GaN and Related Heterostructures in the Context of Devices" in Proc. of Advanced Workshop on 'Frontiers in Electronics' (WOFE) May 31-June 4 (1999) Villard de Lans, France, in press.

Hadis Morkoç "Growth of GaN/AlGaN Modulation Doped and Quantum Well Structures and the Associated Polarization effects", International Conference on Silicon Carbide and Related Materials, October 10-15, 1999, Research Triangle Park, NC. The proceedings papers is by Hadis Morkoç, M. A. Reshchikov, A. Baski, and M. I. Nathan*, "GaN Quantum Dots on Sapphire and Si substrates" Proceedings of the International Conference on Silicon Carbide and Related Materials, October 10-15, 1999, Research Triangle Park, NC USA. Invited.

R. Rinaldi, S. Antonaci, M. Anni, M. Lomascold, R. Cingolani, A. Botchkarev, and H. Morkoç, " Morphological and Optical Characterization of GaN/AlN Heterostructures Grown on Si (111) Substrates by MBE", Phy. Stat. Sol. Vol. 216, pp. 701-706, (1999). Presented at 3rd International Nitride Semiconductor Conference, July 5-9, 1999 Montpellier, France

P. Lefebvre, J. Allegre, B. Gil, A. Kavokine, H. Mathieu, W. Kim, A. Salvador, A. Botcharev, H/ Morkoç "Time-resolved photoluminescence of $GaN/Ga_{0.93}/Al_{0.07}/N$ quantum wells". Nitride Semiconductors Symposium. Mater. Res. Soc. 1998, pp.607-12, Warrendale, PA, USA.

Hadis Morkoç, M. A. Reshchikov, J. Cui, F. Yun, A. Baski, M. I. Nathan, and R. Molnar, "GaN based quantum dot heterostructures", Spring MRS meeting, April 24-27, 2000, San Francisco. Invited.

Appendix A: Epitaxy of AlN layers on sapphire by RF and ammonia MBE

Since the lattice mismatch between sapphire and GaN is very large (>16%) and tendency on the part of GaN to not fully cover the sapphire at high temperatures, an AlN buffer layer is often employed for full coverage and improved GaN layer quality. Therefore, the epitaxy of AlN has become a very critical step along with low temperature GaN buffer layers in the III-Nitride materials development.

AlN MBE has been performed in the Riber 1000 system using only ammonia as nitrogen source as well as at SVT system using active RF nitrogen source and sometimes ammonia. The details of the AlN MBE procedure employed are as follows:

1). Sapphire substrates first undergo a chemical (solvent) cleaning procedure, in which the substrate is dipped in a solution of TriChlorEtane (TCE), kept at 300 °C, for 5 minutes. The substrate is then rinsed for 3 minutes each in acetone and methanol. This procedure is followed by a 3-minute rinse in deionized (DI) water. The above steps are repeated three times to complete the degreasing process.

Following the degreasing procedure, the surface damage is removed by chemical etching. A 3:1 solution of hot H_2SO4: H_3PO_4 (300 °C) is then used for 20 minutes to remove some of the surface material. This is followed by a rinse in DI water for 5 minutes. This procedure serves to remove the surface damage, but does not remove the troughs and morphological features from the surface which impede the layer growth. To circumvent this problem, we developed a high temperature annealing procedure to successfully remove those features. The details of this procedure were discussed in the progress report for the last reporting period. Following this procedure, sapphire substrates were loaded into the growth reactor for the growth experiments.

2). In-situ thermal cleaning of sapphire in the chamber was performed at about 930°C for 20 minutes, then nitridation was initiated using RF nitrogen in the SVT system or by using NH_3 in the Riber system. This process is continued for 30minutes. Some 10

minutes into the nitridation process, the sapphire surface reconstruction changed into AlN structure confirmed by RHEED in the SVT system. The RHEED is 1x1 for both azimuths of AlN and the [112bar0] direction of AlN rotates 30° with respect to the sapphire [112bar0] direction.

3). After the nitridation process, AlN epitaxy was performed at temperatures in the range of about 650°C to 850°C in the Riber system, and in the range of about 850°C to 950°C in the SVT system for high temperature AlN (HT-AlN). The high temperature buffer layers grown with RF, while very smooth, under 0. 5 nm, display incomplete domains. If is for this reason we also explored low temperature buffer layers of GaN and AlN, though we will concentrate on the AlN buffer layers in this appendix. The low temperature AlN buffer layers (LT AlN) were deposited at 530°C. Though excellent, atomically smooth, surface morphologies were obtained, these some 20 nm films before and after high temperature annealing did not exhibit any X-ray diffraction peaks whereas the high temperature ones do so. We need to optimize the parameters some more.

It should be mentioned that the thermal cleaning and nitridation parameters we used here are the optimized parameters and we did not change them during the experiments of AlN growth. AlN layers were characterized by AFM (Digital Nanoscan III), and X-ray diffraction (Philips MRD with 10 are second resolution). The CL measurement was performed at 6K.

In reactive MBE with ammonia nitrogen source, the AlN layers have [002] symmetric X-ray full width at half maximum (FWHM) of as low as 2 to 3 arcmin. When high growth temperature was used. In RF activated nitrogen case, the X-ray full width at half maximum (FWHM) of as low as 1.8 arcmin has been reached, normally the [002] peak has FWHM of about 5 arcmin and [104] asymmetric peak has FWHM of around 10 arcmin. These small FWHM means the AlN have high crystal quality, except the incomplete domain problem mentioned above.

The surface topographical features were investigated by AFM. In the reactive MBE system with ammonia, when the growth temperature is lower, the surface has "ball" like features. These "domains" get larger when the temperature is raised (samples R6210 to R6217) until T_g=830°C is reached where the balls begin to merge to each other and coalesce. The growth tends toward 2D growth at this high temperature and the surface changes into a very smooth one with the RMS for AFM image being just 0.67nm (Sample R6399). Meanwhile, in the RF MBE case, a smoother surface can be obtained in that the RMS for AFM image is about 0.2 to 0.5nm for high temperature grown AlN layers. A low temperature growth has been tried, the AFM image shown a RMS as smaller as 0.1nm after the AlN film was annealed at 800°C for 20min. Again, incomplete domains remain to be the problem.

Cathodoluminescence measurements were performed at 6K for some of the samples investigated. For R6180 sample, which was grown using ammonia, has both [002] and [104] X-ray FWHM as small as about 6 arcmin, respectively. The CL peak (obtained at University of Pittsburgh) located at 6.045eV is identified as band-edge emission and has a FWHM value of 6.25Å. This is smaller than the AlN grown on Si (SVT 127 sample) which has a FWHM value of 13Å. The SVT 288 sample has a its peak at 6.0eV and the FWHM 11.4 Å. Other samples such as R6268 and R6269 have red shifted peaks at 5.96eV with FWHM of 25Å. Beside the band-edge emission peak, there is other peak located at 3.8eV with FWHM of 450Å for sample R6268 and 500Å for sample R6269.

In one of the most recent experiments, we were able to cause step flow growth of AlN to take place in reactive MBE on an AlN grown by RF nitrogen source. The high growth temperature employed changes the AlN growth mode from 3D island formation into 2D step flow, this has been confirmed (Sample R6400). The growth experiment was performed at 850 for 30min leading to a thickness of about 60 nm. An atomically smooth surface has been seen in AFM images with RMS is as smaller as 0.16 nm on a

1micrometer scale scan. The terrace width is about 130 nm with step height of about 0.3 nm, which is just about the bilayer step height of AlN. This kind of surface can be used as a buffer for GaN QD growth.

Appendix B: GaN and GaN/AlGaN MODFET Structures

Discussed below are the particulars, such as mobility and X-ray data, whichever is applicable, of GaN and MODFET structures grown in our laboratory. Samples have been catalogues based on their salient features, which are Quantum Dots, GaN bulk layers, GaN with low-temperature grown AlN or GaN buffer layers, and MODFET structures.

(1) Quantum dots

Sample	x-ray(min) [002]/[104]	thickness (μm)	PL(10K): quantum efficiency (%)	PL(10K): width (meV) / peak position (eV)	time (s) : GaN/AlN
342	1.6/4.4	1.06	6.33	59/3.537	20/40
343	2.1/6.0	0.97	12.3	58/3.536	20/40
344	1.6/2.2	0.76	6.56	62/3.548	20/40
345	1.8/6.1	1.31	3.72	25/3.558	20/40
346	2.0/6.1	0.93	6.6	34/3.546	20/60
347	1.9/6.4	1.05	22.1	69/3.427	30/60
352	1.6/5.8	1.22	5.16	48/3.556	20/60
353	1.6/6.3	1.16	4.91	67/3.550	20/60

All above samples were grown in a SVT MBE system. In this MBE system, both RF plasma and NH_3 can be used to generate nitrogen precursors. Usually, 1 μm GaN is firstly grown using RF plasma, then MQDs structure with 30 periods is grown using NH_3. From x-ray measurement, AlN layer in MQDs structure is partly relaxed in respect to GaN buffer. Above table shows Sample 347 has the largest quantum efficiency. It has the longest GaN growth time among all samples. Although exact growth mechanism is still not clear, previous studies from other laboratories show that when growing GaN on

completely relaxed AlN, first two layers are grown in layer-by-layer growth, next layers exceeding two in island growth. For our partly relaxed AlN, maybe a larger GaN thickness is needed to trigger the island growth, i.e., to form quantum dots.[1] Further studies should make clear the growth mechanism to try to enhance the quantum efficiency. The kinetic effect should considered to form quantum dots when NH_3 is used as nitrogen precursor.[2]

(2) GaN bulk layers

sample	x-ray(min) : [002]/[104]	thickness (μm)	mobility/density	structure	PL(10K): quantum efficiency / linewidth
349	2.0/5.8	0.88	452/7.1e16 (RT) 757/7.5e16 (77K)	1QD	0.14% 23 meV
360	2.0/7.7	0.89	725/6.7e16 (RT) 953/5.5e16 (77K)	1QD	0.07% 15.2 meV
362	1.8/5.8	1.13	1265/8.1e16 (RT) 1700/7.3e16 (77K)	1QD	0.02% 14 meV
369	3.6/6.8	1.2	649/1.53e17 (RT)	2QDs	0.09% 18 meV
375	1.6/5.1	0.93	635/2.0e17 (RT) 829/1.85e17 (77K)	1QD	0.06% 12 meV
381	1.98/5.0	1.19	690/6.61e16 (RT)	1QD	0.05% 11.5 meV
388	1.79/7.52	0.84	741/1.13e17 (RT)	1QD	0.057% 12.7 meV
405	2.32/9.38	1.16	562/1.17e17 (RT)	1QD	0.047% 9 meV
337	8.6/10.2	0.93	92/1.95e17 (RT)	no QD	0.096% 33.4 meV
358	N/A	1.23	45/3.75e15 (RT)	no QD	0.03% 20 meV
374	1.8/6.9	0.82	59/1.0e15 (RT)	no QD	0.04% 13 meV

All GaN bulk samples are grown in SVT MBE system. We have invented a new technique of dislocation blocking. Although there are some differences in details, similar techniques also have been used by others.[3,4] In this technique, by inserting a layer of MQDs structure between top and bottom GaN layers, we can greatly improve the quality of the top GaN layer. From the analysis of many samples, we have the conclusion that the linewidth of the X-ray rocking curve in [10.4] can be greatly decreased in samples with a MQDs buffer layer. Further Hall effect measurement, we find the mobility can be surprisingly improved. For sample 362, at room temperature we measured a mobility of 1265 cm^2/Vs at an electron concentration of $8.1x10^{16}$ cm^{-3}; at 77 K we obtained a mobility of 1700 cm^2/Vs at an electron concentration of $7.3x10^{16}$ cm^{-3}. This is the new record in the mobility of GaN bulk materials. From X-ray, we know that the strain states in top and bottom GaN layers are different. At present, we still do not know clearly the mechanism of the MQDs buffer layer in improving the material quality.

(3) GaN with low-temperature grown AlN or GaN buffer layers

sample	structure	x-ray: [002]/[104]	μ/n (RT)	surface morphology	thickness (μm)	PL
384	LTAlN(a)+GaN	1.92/24	high R	small grains	0.79	green
385	LTAlN(a)+GaN	2.26/28	high R	small grains	0.72	green
410	LTAlN(a')+GaN +LTAlN(a')+GaN	2.36/5.56	20.6 2.24e17	small grains	0.81	green
397	LT nitridation +LTAlN(a)+GaN	2.49/5.33	90.4 5.87e14	large islands	1.52	green
400	LT nitridation +LTAlN(a)+GaN	3.05/15.6	high R	large islands	0.47	green
412	LTAlN(a')+GaN +LTAlN(a')	N/R	N/R	large islands	N/R	N/R
401	LHAlN(a)+GaN	2.10/5.07	high R	horizontal	1.06	green

				columns		
402	LHAlN(a)+GaN	2.20/6.16	high R	horizontal columns	N/R	green
393	LTAlN(u)+GaN +QD+GaN	1.79/4.32	high R	N/R	0.8	broad green
406	LTAlN(a)+GaN +QD+GaN	2.61/7.70	45.7 2.69e17	a lot of troughs	0.9	green
403	HTAlN+GaN +LTAlN(a)+GaN	2.61/9.19	312.5 1.43e18	N/R	N/R	N/R
409	HTAlN+GaN +LTAlN(a')+GaN	1.76/4.79	397 5.12e16	a lot of troughs	1.5	green
404	LHAlN(a)+GaN	2.40/N/A	N/A	N/R	0.16	N/R
407	LHAlN(a)+GaN +QD+GaN	2.87/8.64	233.5 2.34e17	a lot of troughs	0.94	green
408	LHAlN(a)+GaN +QD+GaN	2.78/7.09	282 2.95e17	a lot of troughs	0.83	green
419	HTAlN+GaN +LTGaN(a',a) +GaN	4.99/5.68	N/R	a lot of troughs	N/R	green
420	HTAlN+GaN +LTGaN(u)+GaN	6.47/6.26	N/R	a lot of troughs	N/R	N/R

In above table, the properties of all samples with low-temperature (LT) grown layer are listed. According to the AFM surface morphology, we can classify samples into several types: small grains, large islands, horizontal columns and troughs. The annealing conditions of LT layer are given using different symbols. " a " denotes annealing under RF plasma, " a' " denotes annealing under NH_3 exposure and " u " means no annealing.

In sample 384 and 385, we annealed LT-layer at (18.0A/56.2V) 830 °C for 10 min. Their surfaces show a lot of small grains. Hall measurement points out they are of high resistivity. X-ray measurement finds that they have very broad linewidth of the rocking curve in [10.4]. Increasing annealing temperature to (21.5A/67.8V) 1004 °C and making

annealing under NH_3 can improve mobility and structure quality, as can seen in sample 410. Although their surface morphologies are the same type, in sample 384 and 385 we only can observe 1x1 RHEED pattern at 450 °C, while we obtained 2x2 in sample 410.

Using high annealing temperature of LT AlN nucleation layer, another type of surface morphology: large non-coalesed islands can be observed in sample 397, 400 and 412. For these three samples, only 1x1 RHEED can be obtained at low temperature. Maybe the surface morphology is of mixed polarity.

If after an annealed LT AlN nucleation layer, we grow another AlN layer at high temperature, we can see horizontal columns on the sample surfaces (sample 401 and 402). We obtained 2x2 in sample 401 and 2x1 in sample 402 at low temperature. Hall measurement finds that they are of high resistivity.

Unannealed LT AlN nucleation layer leads to very bad quality of top GaN layer (sample 393). Annealed LT AlN nucleation layer and another buffer layer of MQDs structure can improve sample quality a little bit (sample 406).[5,6] If the AlN nucleation layer consists of an annealed LT layer and then a HT layer (LH AlN), another buffer layer of MQDs structure can improve mobility greatly. However, the sample quality is still not better than those samples without any LT layers. The GaN samples with a LH AlN nucleation layer and a layer of MQDs have very rough surfaces with a lot of troughs. For these samples we obtain weak 2x2 or 2x1 RHEED structures.

Annealing LT layer under NH_3 is better than under RF plasma, this can be seen in sample 403 and 409. When we insert an annealed LT AlN layer in GaN layer with a HT AlN nucleation layer, we also obtain very rough surfaces (sample 409). In contrast to this, inserting a LT GaN layer gives a very broad linewidths for X-ray rocking curves (sample 419 and 420).

All above table-listed samples shows red and green PL bands at 10 K, while most of those samples without LT layer have yellow band in PL spectra. Apparently the red and yellow PL bands are correlated to LT AlN layers. Etching experiments using hot H_3PO_4 shows except for sample 401, 402 and 409, others samples are very easy to etch.

There are still some problems with LT-AlN nucleation layer. Further investigation in growing LT AlN layer should start from the structure of sample. Optimizing growth and annealing conditions of LT AlN layer will improve surface morphology.

(4) MODFET structures

sample	μ/n	x-ray: [002]/[104]	thickness (μm)	structure
350	516/3.6e12 (RT) 622/2.94e12 (77 K)	2.0/5.8	1.06	1QD
351	882/1.4e12 (RT) 1129/1.4e12 (77 K)	2.4/7.7	0.9	2QD
364	725/7.4e12 (RT)	2.4/8.2	1.43	1QD
368	252/9.6e12 (RT)	2.6/6.3	1.28	2QD+ δ doping

392	530/7.1e12 (RT)	1.9/5.62	N/R	1QD
399	322/4.4e12 (RT)	1.92/6.54	0.32	no QD

Through a MQDs buffer layer, we have greatly improved mobility of the bulk GaN materials. Using this technique, we have grown several samples with MODFET structure and fabricated devices. Further optimizing the growth condition of AlGaN layer we can improve mobility greatly.

References:

(1) F. Widmann, B. Daudin, G. Feuillet, Y. Samson, J. L. Rouviere, N. Pelekanos, J. Appl. Phys., 83, 7618 (1998).

(2) S. W. King, E. P. Carlson, R. J. Therrien, J. A. Christman, R. J. Nemanich, R. F. Davis, J. Appl. Phys. 86, 5584 (1999).

(3) D. D. Koleske, M. E. Twigg, A. E. Wickenden, R. L. Henry, R. J. Gorman J.A. Freitas, Jr., and M. Fatemi, Appl. Phys. Lett. 75, 3141 (1999).

(4) S. A. Nikishin, N. N. Faleev, A. S. Zubrilov, V. G. Antipov and H. Temkin, Appl. Phys. Lett. 76, 3028 (2000).

(5) X. H. Wu, D. Kapolnek, E. J. Tarsa, B. Heying, S. Keller, B. P. Keller, U. K. Mishra, S. P. DenBaars, and J. S. Speck, 686, 1371 (1996).

(6)L. K. Li, M. J. Jurkovic, W. I. Wang, J. M. Van Hove, and P. P. Chow, Appl. Phys. Lett. 76, 1740 (2000).

Appendix C: Spontaneous and Piezoelectric polarization effects on the output characteristics of AlGaN/GaN heterojunction Modulation Doped FETs

Fabio Sacconi, Aldo Di Carlo, P. Lugli, and Hadis Morkoç

ABSTRACT

We report on the calculation of electrical characteristics of AlGaN/GaN heterojuction field effect transistors. The model is based on the self-consistent solution of the Schrödinger and Poisson equations coupled to a quasi-2D model for the current flow. Both single and double heterojunction devices are analyzed for [0001] or [000-1] growth directions. The onset of a parasitic p-channel for particular growth directions and alloy concentrations is also shown.

INTRODUCTION

AlGaN/GaN modulation doped- field–effect transistors (MODFETs), also referred to as HEMTs, have recently received considerable attention due to their potential use for high-voltage and high-power operation at microwave frequencies [1]. High peak electron velocity, saturation velocity, thermal stability and breakdown fields are in fact very appealing properties of nitride materials for such applications. High power MODFETs on SiC substrates exhibited [2] a power density of 6.8 W/mm in a 125 μm-wide device and a total power of 4 W (with a power density of 2 W/mm) at 10 GHz. Power devices on sapphire substrates also have enjoyed a steady improvement despite the relatively low thermal conductivity of sapphire. [3] Very recent GaN/AlGaN MODFETs prepared by MBE on SiC substrates exhibited a total power level of 6.3 W with a power added efficiency of 38 % at 10 GHz from a 1-mm wide device. What is more astounding is that the power level is not really thermally limited as the power density extrapolated from a

0.1-mm device is 6.5 W. [4] Equally impressive is the noise figure of about 0.6 dB at 10 GHz with an associated gain of 11 dB. [5]

A unique feature of the AlGaN/GaN material system is the high sheet carrier concentration, which can be achieved in the channel due to large band discontinuities at the interface. In fact, due to the piezoelectric [6] and spontaneous polarization [7], high sheet carrier concentrations can be obtained even without intentionally doping the barrier. This effect is much more pronounced in GaN based heterostructures when grown on the c-plane than in the case of conventional III-V materials. It has been shown that piezoelectric effects can have a fundamental influence on the electron distributions in strained nitride-based wurtzite heterostructures [8-9]. In fact, in AlGaN-based transistors, the piezoelectric polarization of the top layer is more than five times larger than in analogous AlGaAs structures. Furthermore, according to Bernardini et al. [7], a very large spontaneous polarization charge also exists which must be taken in account in the calculations of the sheet carrier concentration [10]. In short, the piezoelectric and spontaneous polarization charge is inextricable from the gate-induced and or charge-induced by doping in FETs, and must be carefully considered in device design and analysis.[11]

In this article we report the results of our calculation of the electrical characteristics of AlGaN/GaN heterostructures, by taking into account of both piezoelectric and spontaneous polarization and considering also the important role of the crystal structure polarity. Sheet carrier concentrations are calculated by means of a coupled solution of Schrödinger -Poisson equation. A quasi-2D model is then used to calculate the I-V characteristics for normal and inverted MODFET configurations.

MODEL AND SELF-CONSISTENT RESULTS

In order to study the mechanisms of channel formation and of current flow in GaN based MODFET, Schrödinger's equation can be used self-consistently coupled with Poisson equation [12].

Several approaches can be used to define the system hamiltonian in the Schrödinger equation, namely envelope function [13], k.p expansion [10] and tight-binding expansion [14,15,16]. The use of sophisticated models such as k.p or tight-binding is justified, perhaps even made necessary, by the complex wurtzite band structure, particularly for determining the valence band states. Consequently, calculations of optical properties related to band to band transitions should consider band structure details beyond the simple effective mass approximation (EMA) [17]. However, as long as only conduction band processes are of interest, EMA still holds. In fact, nitride based semiconductors in the wurtzite structure present a conduction band with a Γ minimum, which can be described reasonably well within such approximation.

Within the effective mass theory, Schroedinger's equation takes the form [13,12,18], :

$$-\frac{\hbar^2}{2}\frac{d}{dz}\left(\frac{1}{m(z)}\frac{d}{dz}\right)\varphi+\left(eV(z)+\Delta E(z)\right)\varphi=E\varphi \qquad (1)$$

where *m(z)* is the position dependent effective mass, *V(x)* the electrostatic potential, *ΔE* the band discontinuity, φ the electron wavefunction and *E* the electron energy. Non-parabolicity may induce deviations from the simple parabolic band model, however this will not substantially change our results.

In the nitride semiconductors grown in the wurtzite structure, the presence of spontaneous and piezoelectric polarization effects implies that Poisson equation has to be solved for the displacement field, *D(z)*

$$\frac{d}{dz}D(z)=\frac{d}{dz}\left(-\varepsilon(z)\frac{d}{dz}V(z)+P(z)\right)=e\left(p(z)-n(z)+N_D^+-N_A^-\right) \qquad (2)$$

where *ε(z)* is the position-dependent dielectric constant, *P* the total polarization, *n(p)* the electron(holes) charge concentration and N_D^+(N_A^-) the ionized donor(acceptor) density. The total polarization charge can be written as $P_{tot}= P_{piezo}+P_{spont}$, where P_{piezo} is the piezoelectric charge caused by the lattice mismatch (mis) and by the thermal strain (ts) [$P_{piezo} = P_{mis} + P_{ts}$], whereas P_{spont} represents the spontaneous polarizability of the GaN/AlGaN interface, as clearly demonstrated by the recent works of Bernardini et al.[7]. The

piezoelectric charge induced by the lattice in-plane mismatch ($\sigma_{\parallel}$) can be calculated as $P_{lm} = -2$ $(e_{33}\frac{C_{11}}{C_{33}} - e_{31})\sigma_{\parallel}$, where e_{ij} and C_{ij} are the piezoelectric tensor components and the elastic constants, respectively, as given in ref.[7]. Since the layers are grown on thick GaN buffer layers, we expect that the GaN layers are relaxed and take the bulk GaN lattice constant of the buffer (3.189 A). Moreover, we assume that the AlGaN layers grow pseudomorphically in our structures and undergo a tensile in-plane strain $\sigma_{\parallel}$. We neglect the thermal strain in our calculations. As far as the spontaneous polarization charge is concerned, we take the recent data of ref.[7], leading to P_{sp}= -0.029 C/m^2 for the GaN and P^b_{sp}= -0.08 C/m^2, for the AlN. The spontaneous polarization for the AlGaN alloy has been obtained by linear interpolation of the binary compound values.

A self-consistent procedure has been set up, where the potential V is obtained using Eq. (2) from an initial guess of the mobile charge concentration, and then inserted into the Schrödinger's equation, (Eq. (1)) which is solved to obtain the energy levels and wavefunctions of the systems. The new electron charge density is then calculated by applying Fermi statistics:

$$n_{2D}(z) = \frac{m(z)k_B T}{\pi\hbar^2}\sum_i |\varphi_i(z)|^2 \ln\left[1 + e^{\frac{E_F - E_i}{k_B T}}\right]$$

where E_F is the Fermi level, E_i the energy of the i-th quantized level, T the temperature and k_B the Boltzmann constant. The calculated density is than plugged into Poisson equation (Eq. (2)) and the iteration repeated until convergence is achieved. Convergence of the self-consistent algorithm can be improved by adopting special relaxation techniques. Here we have used a first order expansion of the model reported in Ref. [19].

In the following, we consider two structures, namely a single heterojunction AlGaN/GaN FET (MODFET) and an "inverted" double heterojunction GaN/AlGaN/GaN FET (DHMODFET). The MODFET structure consists (moving from the gate contact to the substrate) of a 150 Å n-doped (n=10^{18}cm^{-3}) AlGaN layer, a 50

Å unintentionally doped AlGaN region and a thick GaN buffer. The DHMODFET consists of 300 Å unintentionally doped GaN, 50 Å unintentionally doped AlGaN, 150 Å n-doped ($n=10^{18}cm^{-3}$) AlGaN, 300 Å unintentionally doped AlGaN layers on a thick GaN buffer.

We consider a residual doping of 10^{17} cm^{-3} for both GaN and AlGaN layers. We use a Schottky barrier height (ϕ_B) of 1.1 eV for the metal-GaN interface and a ϕ_B=1.2 eV for the metal-AlGaN interface. Calculations have been performed for $Al_xGa_{1-x}N$ regions with Al concentration of x=0.1, 0.2, 0.3, 0.4. Both [0001] and [000-1] growth directions are considered. In the simulations we have used an effective mass of 0.19 for electrons and 1.8 for holes in both GaN and AlGaN layers. Band gaps and band discontinuities of the AlGaN layer as a function of the Al concentration are reported in Table I.

As discussed above, polarization effects are quite important in nitride-based MODFET's. The conduction band edge profile for the MODFET grown along the [0001] direction is depicted in Fig. 1 for the cases *i)* with both spontaneous and piezoelectric polarization fields, *ii)* without considering any polarization field, *iii)* with only the piezoelectric polarization fields. The difference in piezoelectric and spontaneous polarization between AlGaN and GaN layer determines a fixed 2D charge density at the interface between the two materials. For the [0001] growth direction considered in the figure the polarization difference between the two materials induces a positive charge ($\sigma=+1.12x10^{13}$ cm^{-2}) at the $Al_{0.2}Ga_{0.8}N$/GaN interface. Electrons are attracted by this positive charge, and tend to accumulate at the interface, thus forming a conductive channel. Moreover, the high electric field induced by the interface charge, favors the build up of a large channel density and of a strong channel confinement. Within the AlGaN layer, the strong electric field compensates the space charge contribution coming from the ionized donors. Consequently, it prevents the appearance of the parasitic channel that would otherwise form if a high doped AlGaN layer is considered. [10,20].

The three curves corresponding to different contributions of the polarization fields shown in Fig 1. demonstrate the importance of both spontaneous and piezoelectric polarization in GaN based device operation. In fact, by neglecting the spontaneous polarization, as was done for instance in [9,21-23], leads to an underestimation of the electron channel density [10]. Clearly the sign of the polarization charge is crucial. For the same MODFET structures grown in the [000-1] direction, the resulting polarization charge would be negative (with the same magnitude) and electrons would be repelled from the channel. As we will show later this will lead to a parasitic p-channel formation.

The distribution of the free electron charge in the channel is shown in Fig. 2 for several values of the Al concentration of the AlGaN layer. Increasing the Al content induces a larger polarization charge at the GaN/AlGaN interface and consequently a higher channel electron concentration.

The calculations we have shown so far have been obtained by considering only the polarization charge at the AlGaN/GaN interface. In reality, however, polarization charges that form at the metal-AlGaN and at the end of the GaN buffer region should be also accounted for. The metal-AlGaN charge is completely screened by the charges induced on the metal surface and can therefore be neglected. On the other hand, the charges at the end of the buffer region may have a strong effect. Oberuber et al. [10] considered a $-\sigma/2$ charge at the interface between the GaN and a nucleation region. The exact amount of such charge depends, however, on the morphology of the heterojunction and may differ from the expected value $\sigma=\Delta P/\varepsilon$. The situation is less critical if the bottom interface is far away from the main AlGaN/GaN heterojunction. In this case, the polarization charge that arises can be completely screened by the residual doping of the GaN substrate. On the contrary, if such interface is close to the AlGaN/GaN heterojunction, the polarization charge can completely deplete the channel. In our simulations we have considered a thick GaN substrate. Thus, the effect of the polarization charge at the end of the GaN substrate is completely screened.

The band edge profile and electron densities for the DHMODFET grown in the [000-1] direction are shown in Fig. 3 and Fig 4, respectively. A comparison of the conduction band edges with and without polarization charges is also plotted. As for the MODFET, the presence of the fixed and positive polarization charge at the GaN/AlGaN interface induces the formation of a channel, which is not present in the absence of the polarization charge. For the DHMODFET, a $-\sigma$ polarization charge is also present at the end of AlGaN region (i.e. at the AlGaN/GaN interface). Similarly to the [0001] grown MODFET, a larger Al content of the AlGaN layer induces a larger polarization charge at the GaN/AlGaN interface and consequently an increase of electron concentration in the channel. Clearly, for [0001] orientation the interface-charge forms below the AlGaN layer which is not desirable for an inverted DHMODFET. Rather, the formation of the electron sheet layer on top of the AlGaN layer is preferable, which requires the [000-1] orientation. The structure in its present shape, i.e., the [0001] polarity would show FET performance providing that the AlGaN layer is completely depleted but with small transconductance. For gate biases not sufficiently large to deplete the AlGaN, the device would function as MESFET dominated by transport in the AlGaN layer. To eliminate the formation of an interface electron charge at the bottom of the AlGaN layer, the bottom heterointerface should be graded substantially. In that case, the [0001] polarity would cause the band diagram to accumulate holes at the top interface, if they are present. That top interface would accumulate electrons in the [000-1] polarity.

The channel charge density is therefore controlled by two factors: i) the gate bias as in traditional MODFET device, ii) the Al content of the AlGaN layer, which tailors the polarization field. Charge control in nitride-based devices can be achieved by adjusting two independent parameters and thus with a larger degree of flexibility with respect to traditional devices

THE PARASITIC P-CHANNEL

It is well known in heterojunctions that, if a negative fixed polarization charge is induced, an electron depletion region is created. Specific to AlGaN/GaN system is the fact that a parasitic p-channel may originate at the interface depending on the structure of the device. As shown in Figs. 5 and 6, we have calculated the band edge profile and the charge density for a [000-1] grown MODFET and for a [000-1] grown DHMODFET, both with x(Al) = 0.2. In the latter case, both n-channel and p-channel are present in the same structure. In order to determine the conditions for the onset of the p-channel, we have calculated the minimum AlGaN layer thickness as a function of the alloy concentration to achieve the formation of the p-channel in the DHMODFET. We obtain that there is a critical thickness for the heterostructure, beyond which a p-channel forms, and holes must be considered in the calculations. The critical thickness depends on the value of Al concentration in the barrier and, as shown in Fig. 7, it is inversely proportional to x(Al). This behavior is expected considering that a p-channel forms as soon as the electric field ($F \sim \sigma/\varepsilon$) produces a potential drop of the order of the band gap, $eFd \sim Eg$ where d the layer thickness. The calculations assume equilibrium conditions, which in turn requires that holes must be provided by a variety of pathways such as injection from contacts and generation. We must point out that there has so far been no experimental reports of polarization-induced p-channel formation in these structures.

CURRENT MODEL IN MODFET

We have implemented a quasi-2D [24-27] model for the calculation of the current-voltage characteristics of the nitride FETs. This model makes use of the exact value of the sheet charge density in a MODFET device channel, obtained from the self-consistent Schrödinger-Poisson solution presented above.

We use the FET model shown in Fig. 8 where the x-axis is along the channel and the z-axis is along the growth direction. The model also considers the presence of a drain (R_D) and source (R_S) resistance. When a

drain bias (V_D) is applied, the potential along the channel may be considered to vary gradually from the source to the drain. In this situation it is possible to calculate the sheet charge density n_s

$$n_s(V) = \int n(V,z)dz$$

in different sections of the channel, provided that one considers the proper potential V(x) (on the top surface). Since generally V_D is positive, while V_S is zero, V(x) contributes to the channel depletion and the sheet charge density n_s for the generic *x* section of the FET will therefore be:

$$n_s(x) = n_s(V_G - V(x))$$

By neglecting diffusion contributions, the source-to-drain current I_{DS} is given by:

$$I_{DS} = -qWv(x)n_s(x) \qquad (3)$$

where *W* is the gate width and *v(x)* the electron mean velocity, taken independent from the transverse coordinate.

The drift velocity dependence on the longitudinal electric field is given by:

$$v(x) = \frac{\mu_0 F(x)}{1 + \frac{F(x)}{F_C}}$$

where *F(x)* is the electric field (= *dV(x)/dx*), μ_0 is low field mobility and $F_c = v_{sat}/\mu_0$ is the electric field at saturation. Parasitic components are included explicitly through the value of the drain and source resistance (R_D, R_S)

$$V_S^e = V_S + I_{DS}R_S$$
$$V_D^e = V_D - I_{DS}R_D$$

where V^e_D and V^e_S are the effective bias boundary of the gate region.

For a given value of I_{DS}, we can calculate the corresponding V_D by solving Eq. (3).

The explicit equation for the current is:

$$I_{DS} = qW \frac{\mu_0 F(x)}{1+\frac{F(x)}{F_C}} n(V_G - V(x))$$

The numerical solution is based on the discretization of this expression on a number N of sections, each one with amplitude h, so that Nh=L, where L is the gate length. Given the *(i-1)*-th section potential, the *i*-th potential $V_i = V_{i-1} + F_i h$ where F_i is the *i*-th section electric field. We have then N relations:

$$I_{DS} = qW \frac{\mu_0 F_i}{1+\frac{F_i}{F_C}} n(V_G - V_{i-1} - F_i h)$$

Since the *(i-1)*-th section potential is known from the previous step, this is a non-linear equation in the unknown F_i. Solving iteratively for all the N sections, one obtains the value of drain voltage V_D consistent with the assumed current.

Repeating this procedure for a suitable range of values of I_{DS}, one obtains the set of corresponding V_{DS} values and builds the device I-V characteristics.

I-V CHARACTERISTICS

In this section we report the simulated I-V characteristic of the normal and inverted MODFET, obtained for a gate length L=0.3 μm. We have chosen a drain and source contact resistivity of about 1 Ω·mm which is consistent with experimental measured values on these devices [28]. We use a saturation velocity of 2.5 x 10^7 cm/s [29], while for the low field mobility we choose a value of μ_0=1100 cm^2/Vs, slightly higher than the GaN bulk value, according to the experimental and theoretical results for similar devices [10,29-31].

In figure 9 we show the I_{DS} vs V_{DS} for the [0001] grown MODFET, for several gate (V_{GS}) biases. The results are presented for both x=0.2 (Fig. 9a) and x=0.4 (Fig. 9b) Al concentration of the top layer. For x=0.2 the MODFET reaches the pinch-off for a bias of V_{GS}=-4.4V, while for x=0.4 the pinch-off is reached at V_{GS}=-9.5 V. On the other hand, the saturation drain current for x=0.2 is I_{DS}= 2.4 A/mm at V_{GS}=0 and it increases up to 5.76 A/mm for an Al content of x=0.4. Thus, the current flowing in the devices depends strongly on the Al content of the top layer. This is essentially due to the increasing of the channel electron density induced by the enhanced polarization charge when going from an Al contents of 0.2 up to 0.4. This peculiarity of the MODFET should be considered in the design of these devices since fluctuation of the alloy composition of the top layer may induce large variation with respect to nominal electrical values of the device. It should also be pointed out that the gate leakage would determine the extent of gate voltage that can be applied to the gate contact. For a gate bias of 9.5 V and AlGaN layer thickness of 20 nm, the vertical field under the gate near the source can reach 4.75 MV/cm. This means that MODFETs utilizing large mole fractions of Al may require thin AlGaN layers or recessed gates to keep the gate voltage smaller. A similar situation is obtained for the inverted MODFET with GaN/AlGaN/GaN structure grown in the [000-1] direction. The calculated I_{DS} vs. V_{DS} characteristics are reported in Fig. 10 a,b for both x=0.2 and x=0.4 Al composition of the AlGaN layer, respectively. Also in this case the pinch-off bias depends critically on the Al composition and varies from -3.9 V for x=0.2 up to –9.0 for x=0.4. Saturation currents are lower for the DHMODFET at x=0.2 with respect to the equivalent MODFET structure. Such difference, however, is negligible for the case with x=0.4.

I-V characteristics have been also simulated for the inverted AlGaN/GaN structure of Fig. 5. As we have seen, in this case a p-channel is present at the AlGaN/GaN interface and the current flowing in the device is due to the channel hole density.

The calculated I_{DS} vs. V_{DS} characteristics are reported in Fig. 11 for an inverted MODFET with x(Al) = 0.1 and for several negative gate biases. The MODFET reaches the pinch-off for a bias around $V_{GS} = 0$, while the saturation current is around 0.35 A/mm for $V_{GS} = -4$ V.

CONCLUSIONS

GaN-based heterojunction field effect transistors have been investigated by self-consistent schemes and current characteristics have been obtained by means of a quasi-2D approach. The profound influence of the polarization field on the electrical characteristics has been shown. We have demonstrated that a parasitic p-channel can form depending on the growth direction and alloy content. This work was partially supported by the Italian MURST. H. Morkoç is funded by grants from ONR, AFOSR and NSF.

Figure Captions

Fig. 1. Conduction band edge for the MODFET structure grown in the [0001] direction for V_G=0 with and without polarization fields.

Fig. 2. Electron density distribution in the channel of the [0001] grown MODFET for V_G=0 for several Al contents of the $Al_xGa_{1-x}N$ layer.

Fig. 3. Conduction band edge for the DHMODFET structure grown in the [000-1] direction for V_G=0 with and without polarization fields.

Fig. 4. Electron density distribution in the channel of the [000-1] grown DHMODFET for V_G=0 for several Al contents of the $Al_xGa_{1-x}N$ layer.

Fig. 5. Band edges (solid lines) and channel-hole density (shaded region) for the MODFET structure grown in the [000-1] direction.

Fig. 6. Conduction band edge and electron and hole densities for the DHMODFET structure grown in the [000-1] direction.

Fig. 7. Critical thickness of the AlGaN layer in a [000-1] gown DHMODFET for the onset of the p-channel .

Fig. 8. Schematic representation of the quasi-2D FET model used.

Fig. 9. Calculated I_{DS} vs V_{DS} characteristics for the [0001] grown MODFET with a) $Al_{0.2}Ga_{0.8}N$ layer b) $Al_{0.4}Ga_{0.6}N$ layer.

Fig. 10. Calculated I_{DS} vs V_{DS} characteristics for the [000-1] grown DHMODFET with a) $Al_{0.2}Ga_{0.8}N$ layer b) $Al_{0.4}Ga_{0.6}N$ layer.

Fig. 11. Calculated I_{DS} vs V_{DS} characteristics for the [000-1] grown p-channel MODFET with $Al_{0.1}Ga_{0.9}N$ layer

TABLE I Band Gap and Conduction band discontinuities with respect to GaN of the $Al_xGa_{1-x}N$ layer

x(Al)	E_G [eV]	ΔE_C [eV]
0.1	3.62	0.17
0.2	3.85	0.33
0.3	4.09	0.51
0.4	4.35	0.69

REFERENCES

[1] For a complete review see: O. Ambacher, "Growth and applications of Group III-Nitrides", J. Phys. D: Appl. Phys. Vol 31, pp. 2653-2710, (1998):S. J. Pearton, J. C. Zolper, R. J. Shul, and F. Ren, "GaN: Processing, defects, and devices", J. Appl. Phys. Vol. 86, pp. 1-78, (1999); H. Morkoç, "Beyond SiC! III-V Nitride Based Heterostructures and Devices," in SiC Materials and Devices, Y. S. Park, ed., Academic Press, Willardson and Beer Series, eds. Willardson and Weber, Vol. 52, Chapter 8, pp. 307-394, 1998.

[2]S. T. Sheppard, K. Doverspike, W. L. Pribble, S. T. Allen, J. W. Palmour, L. T. Kehias and T. J. Jenkins, "High Power Microwave GaN/AlGaN HEMTs on Semi-insulating Silicon Carbide Substrates," IEEE Electron. Dev. Lett., 20(4), 161, (1999)

[3] Y.-F. Wu, B. J. Thibeault, B. P. Keller, S. Keller, S. P. Denbaars, and U. K. Mishra, "3-Watt AlGaN/GaN HEMTs on Sapphire Substrates with Thermal Management by Flip-chip Bonding," presented at 56th Annual Device Research Conference, University of Virginia at Charlottesville, VA, 1998.

[4]N. X. Nguyen, M. Micovic, W-S. Wong, P. Hashimoto, L.-M. McCray, P. Janke, and C. Nguyen, "High Performance Microwave Power GaN/AlGaN MODFETs Grown by RF-Assisted MBE" Electronics Letters, in press.

[5] N. X. Nguyen, M. Micovic, W-S. Wong, P. Hashimoto, L.-M. McCray, P. Janke, and C. Nguyen, private communication.

[6]A. D. Bykhovski, V. V. Kaminski, M. S. Shur, Q. C. Chen, and M. A. Khan, "Piezoresistive Effect in Wurtzite n-type GaN," Appl. Phys. Lett. 68, 818-819, (1996).

[7] F. Bernardini, V. Fiorentini, and D. Vanderbilt, "Spontaneous Polarization and Piezoelectric Constants in III-V Nitrides," Phys. Rev. B 56, R10024, 1997

[8] O. Ambacher, J. Smart, J.R. Shealy, N.G. Weimann, K. Chu, M. Murphy, W.J. Schaff, L.F. Eastman, R. Dimitrov, L. Wittmer, M. Stutzmann, W. Rieger, and J. Hilsenbeck, "Two-dimensional electron gases by spontaneous and piezoelectric polarization charges in N- and Ga-fase AlGaN/GaN heterostructures", J. Appl. Phys. 85, 3222 (1999);

[9] E.T.Yu, G. J. Sullivan, P. M. Asbeck, C. D. Wang, D. Qiao, S. S. Lau, "Measurament of the piezoelectrically induced charge in GaN/AlGaN heterostructure field-effect transitors", Appl. Phys. Lett. 71, 2794 (1997)

[10] R. Oberhuber, G. Zandler, and P. Vogl, "Mobility of two-dimensional electrons in AlGaN/GaN modulation doped field-effect transistors" Appl. Phys. Lett. 73, 818 (1998).

[11] H. Morkoç, R. Cingolani, and B. Gil, "Polarization Effects in Nitride Semiconductor Device Structures, and Performance of Modulation Doped Field Effect Transistors" Solid State Electronics, vol.43, no.10, pp.1909-1927, Oct. 1999

[12] H. Morkoc, H. Unlu, G. JI, "Principles and technology of MODFETS", Wiley Chichesters, England (1991)

[13] G.Bastard, in "Wave Mechanics Applied to Semiconductor Heterostructures", Edition de Physique, Paris , France, 1987

[14]A. Di Carlo, S. Pescetelli, M. Paciotti, P. Lugli, and M. Graf, "Self-consistent tight-binding calculation of electronic and optical properties of semiconductor nanostructures Solid State Comm. 98, 803 (1996); A. Di Carlo, "Semiconductor Nanostructures" Phys. Status Solidi, 217, 703 (1999)

[15]. F. Della Sala, A. Di Carlo, P.Lugli, F.Bernardini, V.Fiorentini, R.Scholz, and J.M.Jancu, "*Free-carrier screening of polarization fields in wurtzite GaN/InGaN laser structures* "Appl. Phys. Lett., 74, 2002 (1999).

[16] V. Fiorentini, F. Bernardini, F. Della Sala, A. Di Carlo, and P. Lugli "Effects of macroscopic-polarization built-in electrostatic fields in III-V nitrides multi-quantum-wells" Phys. Rev. B 60, 8849 (1999).

[17]. R. Cingolani, A. Botchkarev, H. Tang, H. Morkoç, G. Coli', M. Lomascolo, A. Di Carlo, F. Della Sala, P. Lugli, "Spontaneous polarization and piezoelectric field in GaN/$Al_{0.15}Ga_{0.85}N$ quantum wells: impact on the optical spectra". Phys. Rev. B 61, 2711 (2000) ; A. Bonfiglio, M. Lomascolo, G. Traetta, R. Cingolani, A. Di Carlo, F. Della Sala, P. Lugli, A. Botchkarev, H.

Morkoc, "Well width dependence of the ground level emission of GaN/AlGaN quantum wells ", J. Appl. Phys. 87, 2289 (2000).

[18] P. Lugli, M. Paciotti, E. Calleja, E. Munoz, J.J. Sanchez-Rojas, F. Dessenne, R. Fauquembergue, J.L. Thobel, and G. Zandler: ``HEMT Models and Simulations", in ``Pseudomorphic HEMTs: Technology and Applications", Eds. R. Lee Ross, S. Swensson and P. Lugli, Kluwer Press, pp.141-163,Dordrecht, 1996.

[19] A. Trellakis, A. T. Halick, A. Pacelli, and U. Ravaioli, "Iteration scheme for the solution of the two dimensional Schrödinger-Poisson equations in quantum structures", J. Appl. Phys. 81, 7880 (1997)

[20] K. Lee, M.S. Shur, T.J. Drummond and H. Morkoç, "Parasitic MESFET in (Al,Ga)As/GaAs Modulation Doped FETs and MODFET Characterization," IEEE Trans. Electron. Dev., Vol. ED-31, pp. 29-35, (1984).

[21] P. Ramvall, Y. Aoyagi, A. Kuramata, P. Hacke, K. Horino "Influence of a piezoelectric field on the electron distribution in a double GaN/$Al_{0.14}Ga_{0.86}N$ heterojuction", Appl. Phys. Lett. 74, 3866 (1999).

[22] R. Gaska, J. W. Yang, A. Osinsky, A. D. Bykhovski, M. S. Shur, "Piezoeffect and gate current in AlGaN/GaN high electron mobility transistors", Appl. Phys. Lett. 71, 3673 (1997).

[23] R. Gaska, J. W. Yang, A. Osinsky, A. D. Bykhovski, M. S. Shur, V. V. Kaminski, S. M. Soloviov, "The influence of the deformation on the two-dimensional electron gas density in GaN-AlGaN heterostructure", Appl. Phys. Lett. 72, 64 (1998)

[24] B. Carnez, A. Cappy, A. Kaszynski, E. Constant, G. Salmer, "Modelling of a Submicrometer Gate Field Effect Transistor Including Effects of Nonstationary Electron Dynamics", J. Appl. Phys. 51, 784-790 (1980)

[25] A. Cappy, A. Vanoverschelde, M. Schortgen, C. Versnaeyen, G. Salmer, "Noise Modeling in Submicrometer Gate Two-Dimensional Electron-Gas Field Effect Transistor", IEEE Trans. Electron Dev.,ED-32, 2787-2796 (1985)

[26] P. A. Sandborn J.R. East, G. I. Haddad, "Quasi-Two-Dimensional Modelling of GaAs MESFET's", IEEE Trans. Electron Dev., ED-34, 985-991 (1987).

[27] C. M. Snowden, R.R. Pantoja, "Quasi-Two-Dimensional modelling MESFET simulation for CAD", IEEE Trans. Electron Dev., ED-36, 1564-1573 (1989).

[28] H. Morkoc: "GaN-Based Modulation Doped FETs and UV detectors", Naval Research Reviews 51, 1 (1998)

[29] U. V. Bhapkar, M. S. Shur, "Monte Carlo calculation of velocity-field characteristics of wurtize GaN", J. Appl. Phys 82, 1649 (1997).

[30] M. J. Murphy, B. E. Foutz, K. Chu, H Wu, W. Yeo, W. J. Schaff, O. Ambacher, L. F. Eastman, T. J. Eustis, R. Dimitrov, M. Stutzmann, W. Rieger, "Normal and Inverted AlGaN/GaN based piezoelectric field effect transistors grown by plasma induced molecular beam epitaxy", MRS Internet J. Nitride Semicond. Res. 4S1, G8.4 (1999)

[31]Y.F. Wu, B. P. Keller, S. Keller, D. Kapolnek, P. Kozodoy, S. P. Denbaars, and U.K. Mishra, "Very high breakdown voltage and large transconduttance realized on GaN heterojunction field effect transistors", Appl. Phys. Lett. 69, 1438 (1996).

Appendix D: Defect Characterization by Photoluminescence

Background

The interest to defects in wurtzite GaN is generated by requirement to grow high purity material devices. Photoluminescence (PL) is on of the main methods of study of point defects in GaN. Yet many investigations have been carried out, still the identity and characteristics of defects even in undoped GaN are not well established. The defects in undoped GaN, revealed by PL, can be arbitrarily classified into two groups: (i) defects with strong electron-phonon coupling, which are responsible for broad PL bands at photon energies below 3 eV and (ii) defects with weak electron-phonon coupling giving rise to PL peaks at photon energies above 3 eV. From the first group, a broad band with a maximum at about 2.2-2.3 eV, a so-called yellow luminescence (YL) band is omnipresent in undoped GaN samples grown by different techniques. After hot debates on the type of transitions resulting in YL and the nature of associated defect most of investigators attributed the YL to a deep acceptor, presumably gallium vacancy (V_{Ga}) or its complex with shallow donors ($V_{Ga}Si_{Ga}$ and $V_{Ga}O_N$). A broad band at about 2.9 eV, a blue luminescence (BL) band, is often observed in undoped GaN samples grown by MOCVD and HVPE methods (see Ref. 1 and references in it). It is related to less deep acceptor, however the identity of the defect remains uncertain. A broad PL band with a maximum at about 2.5 eV is much less common in undoped GaN samples. It has been attributed to a deep acceptor of unknown nature [2]. It is widely believed that broad PL bands are related to broad distribution of defect states in the gap. However it is well known that the strong electron-phonon coupling, typical of deep defects, is responsible for large bandwidth of the related PL [3]. Interaction between defects can play secondary role resulting in additional broadening and/or shift of PL band. One should note that potential fluctuations caused by high concentration of charged defects or other reasons can essentially broaden and shift the PL band as it was observed in Mg-doped GaN [4]. Recently it was demonstrated that broad PL bands in GaN can be perfectly explained in terms of the configuration coordinate model and do not require assumption of broad distribution of the defect states in the gap [1,2].

Among the shallow defects or defects responsible for PL peaks in the photon range 3.0 – 3.45 eV, the most widespread and studied is a sharp peak at about 3.27 eV followed by several phonon replicas which is related to the shallow donor-acceptor pair (DAP) transitions [5]. A series of sharp peaks, which are related neither to the shallow DAP nor to the free or weakly bound excitons and their phonon replicas, sometimes are present in the 3.0-3.45 eV range of the spectrum [6, 7]. The origin of these peaks is not clear, yet assumptions have been made that they are related to excitons bound to structural defects [7] and/or some very shallow acceptor [6]. One should remember that in this spectral range the peaks due to artificial effects, such as reflected laser light and fluorescence of the oil vapor, can contribute to the PL spectrum.

An artificial broadening and shift of PL bands can be caused by overlap between several bands related to different defects. Different PL bands may have different behavior with variation of temperature, excitation intensity or other external factors. Therefore the study and classification of various PL bands in the samples with different dominant peaks is of great importance for interpretation of PL spectra.

Results of study

We have studied PL from more than 200 undoped samples grown by reactive MBE method in RIBER and SVT set-ups. Some of samples reveal a set of PL bands typical of the perfect samples. Examples are given in Figs. 1 and 2.

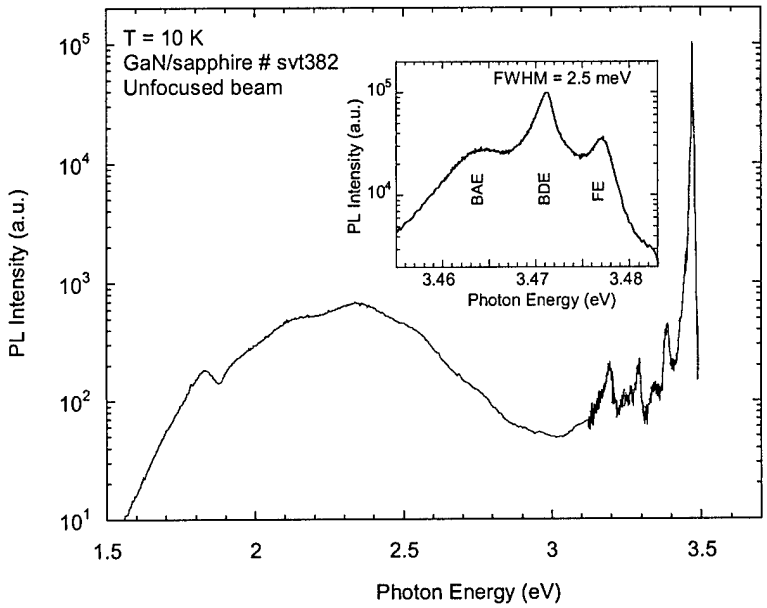

Fig. 1. PL spectrum of a good sample grown in SVT set-up. The long-range modulation of the YL band is due to interference effect. A feature at about 1.9 eV is artifact introduced by using of M250 grating.

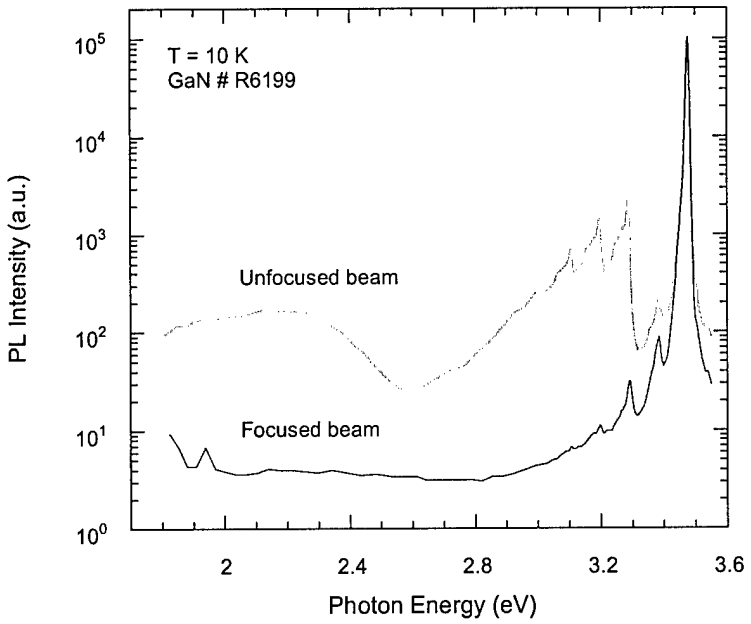

Fig. 2. PL spectrum of a good sample grown in RIBER set-up. The spectra are normalized at peak intensity. Sharp peaks at 3.292 eV and 3.384 eV are LO phonon replicas of the main exciton peak at 3.476 eV (FWHM = 7 meV). Note that the defect PL bands disappear at high excitation density (focused beam) due to saturation of the defect related PL.

The quantum efficiency of PL from the samples grown in RIBER set-up was typically very high (5% for the sample shown in Fig. 2). This presumably confirms low concentration of nonradiative defects in these samples. Most of the SVT-grown samples had much lower quantum efficiency. A good point of the samples grown by SVT set-up is very low contribution of the shallow DAP band (it was not detected in most of the SVT-samples) which can reflect low concentrations of the shallow acceptors and donors.

However some of the samples revealed not typical PL bands which may arise from defects formed due to not optimal conditions of growth. The study of these bands is of particular interest in the samples where they dominate. These defects may also present in smaller amount in good samples but remain invisible because of competing mechanisms of recombination and overlap with other bands. Examples of PL spectra with unusual defect PL bands are shown in Fig. 3.

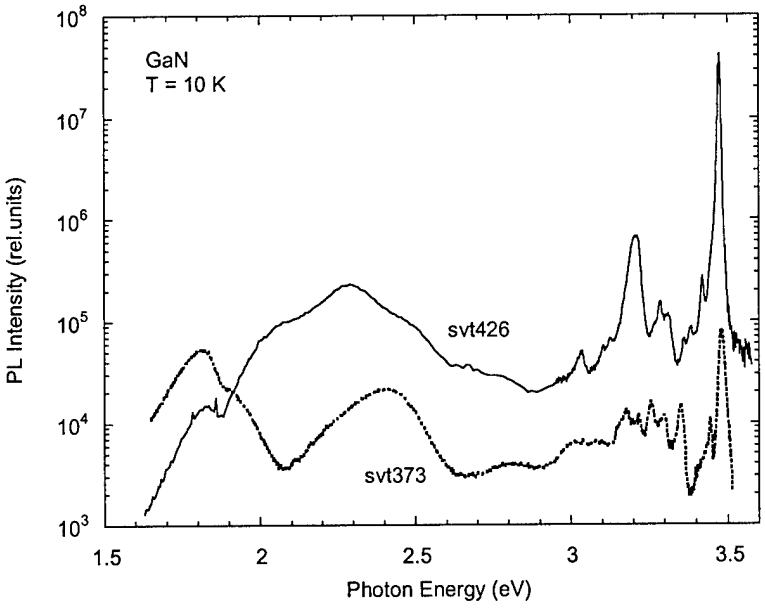

Fig. 3. PL spectra from the samples grown in SVT set-up. Different sources of nitrogen were used: ammonia (sample svt426) and RF plasma (sample svt373).

From the well-known PL bands, only bound to donor exciton with a peak at about 3.47 eV and a YL band (for the sample svt426) can be identified in the spectra shown in Fig. 3. At photon energies below 3.0 eV two broad bands with maxima at about 1.8 eV and 2.4 eV are present, which we will call correspondingly red and green bands due to color of PL. These bands were observed in many samples grown with RF plasma as nitrogen source. In some samples they were not revealed as separate peaks, however probably contributed to the spectrum causing the broadening of the YL emission. In the range 3.0-3.5 eV, several sharp peaks of unknown origin are present. The strongest peak in this range is observed at 3.2 eV in the sample svt 426. The origin of the broad bands and sharp peaks is unknown and not studied. As will be shown below, the study of deep defects responsible for the green and red PL bands can shed light upon the fundamental problem of nonradiative recombination in GaN.

First important point to be noted is that position and shape of the red and green PL bands were nearly the same in large set of samples revealing these bands as separate peaks. They are essentially narrower (FWHM = 220-250 meV) than the YL and as will be shown below their behavior with temperature variation is very different from the known PL bands. Reproduced in many samples shape, position and temperature behavior suggest that some point defects are responsible for this PL rather than a set of defects with distributed states in the gap.

We studied the effect of excitation intensity of the red and green PL bands. Fig. 4 demonstrates PL spectrum for one of the samples recorded at different excitation densities.

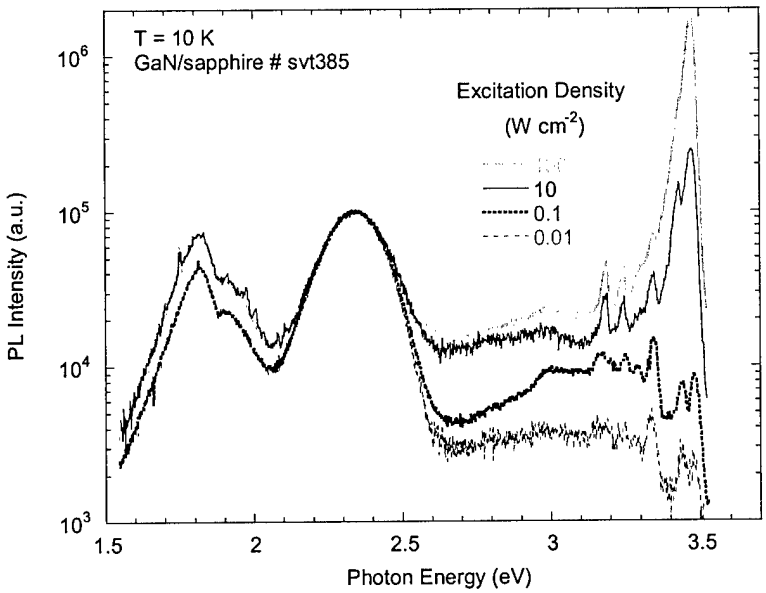

Fig. 4. PL spectrum of a sample grown in SVT set-up with RF plasma as nitrogen source. Spectra are normalized at maximum of the green band. No shift of red and green band with excitation power has been observed with accuracy of 5-10 meV. Sharp peaks at 3.185, 3.244, 3.345 and 3.430 eV are due to reflected laser light. Exciton peak at about 3.47 eV rises superlinearly with excitation power.

Variation of excitation intensity can reveal if the transition of the DAP nature or not. DAP with deep donor are characterized by enormous shift of PL band with excitation intensity when the latter is varied in large range [4]. This shift is related to strong Coulomb interaction in pairs with small separation, which recombine much faster than the long-distance pairs. Saturation of PL from the long-distance pairs with excitation power is responsible for this effect [4]. In case of red and green bands no shift with accuracy of 5-10 meV has been observed when the excitation density was varied in very large range. This suggests that transitions responsible for the observed PL bands involve deep acceptors and possibly shallow donors (the shape, position and behavior of the broad band will be nearly the same in cases of DAP type transitions involving a shallow donor and transitions from the conduction band to the same acceptor because all important properties of both types of transitions are defined by acceptor with strongly localized hole). We can exclude possibility of transition from a deep donor to the valence band. Indeed, such type of transition is quite improbable in n-type GaN due to high rate

of the holes escape from the valence band and typically low hole-capture cross-section of deep donors. As may be seen from Fig. 4, the relative contribution of the exciton emission greatly increases with excitation power. Variation of the quantum efficiency of the red, green and exciton bands with excitation density is shown in Fig. 5.

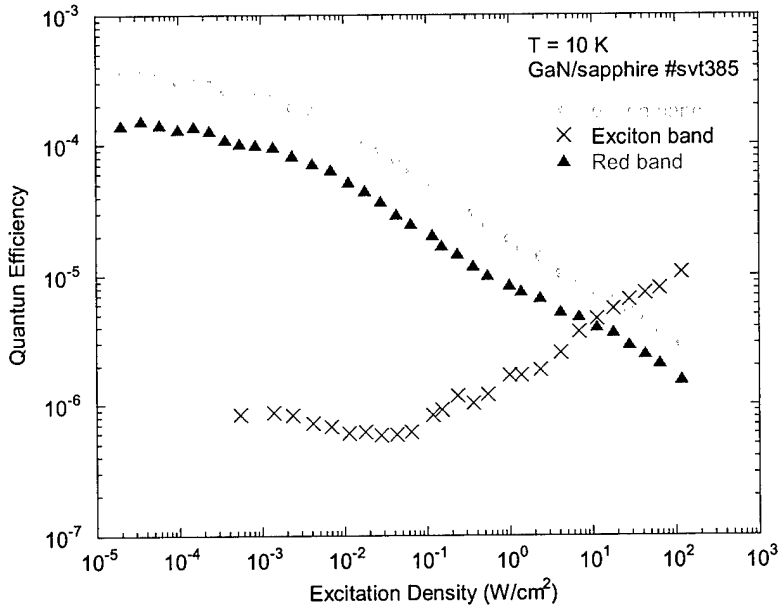

Fig. 5. Quantum efficiency of PL bands versus excitation density of incident light.

It is evident that PL intensity of the red and green bands comes into saturation at excitation density above about 1 mW cm^{-2}. This effect may be related to limited concentration of the acceptors responsible for these PL bands and large lifetime of optical transitions. To estimate quantitatively the concentration of the defects, one should find the lifetime of PL from the transient PL study. An increase of quantum efficiency of the exciton emission above 100 mW cm^{-2} can be explained by predominance of the photogenerated electrons over equilibrium electrons in the conduction band in this excitation range.

We have studied the effect of temperature on the red and green PL bands. Intensity of the green PL band remained unchanged up to 100 K, then a thermal quenching with activation energy of 120-140 meV has been observed, see Fig. 6. Intensity of the red band increased in the temperature range 10-60 K with activation energy 1.2 meV, then a thermal quenching with activation energy of 120-140 meV has been observed (Fig. 6). The temperature dependencies of the PL intensity can be fitted by the following expression

$$I_{PL} = \frac{A\exp(E_1/kT)}{1+B\exp(E_2/kT)}\ , \qquad (1)$$

where A and B are constants and E_1 and E_2 are activation energies.

These dependencies were reproduced on many samples. It is interesting to note that both red and green PL totally disappeared at room temperature. This is very different from behavior of other deep defects in GaN. So, intensities of the yellow (2.2 eV) and green-blue (2.5 eV) broad bands come to thermal quenching only above 500 and 300 K

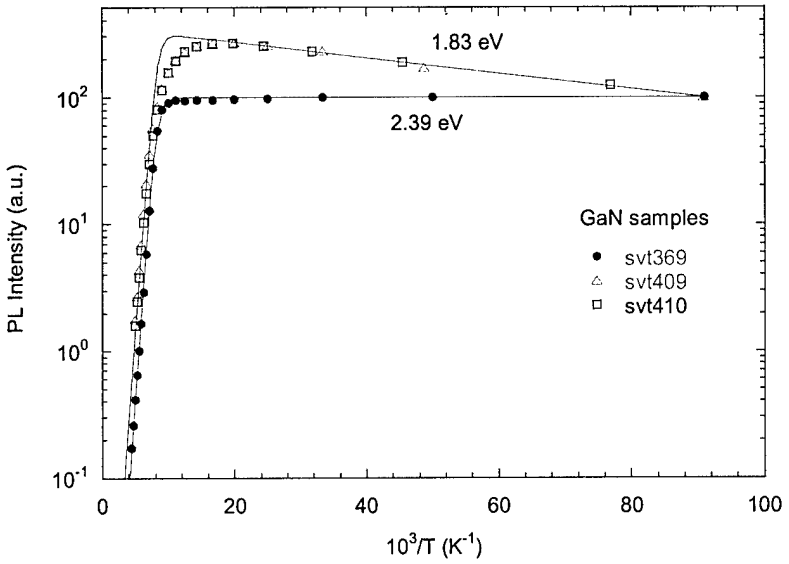

Fig. 6. Variation of PL intensity for the red (1.83 eV) and green (2.39 eV) bands in undoped GaN samples. Points are experimental data. The solid curves are calculated using Eq. (1) with the following activation energies: $E_1 = 0$ and 1.2 meV for the green and red bands respectively; $E_2 = 140$ meV for both bands.

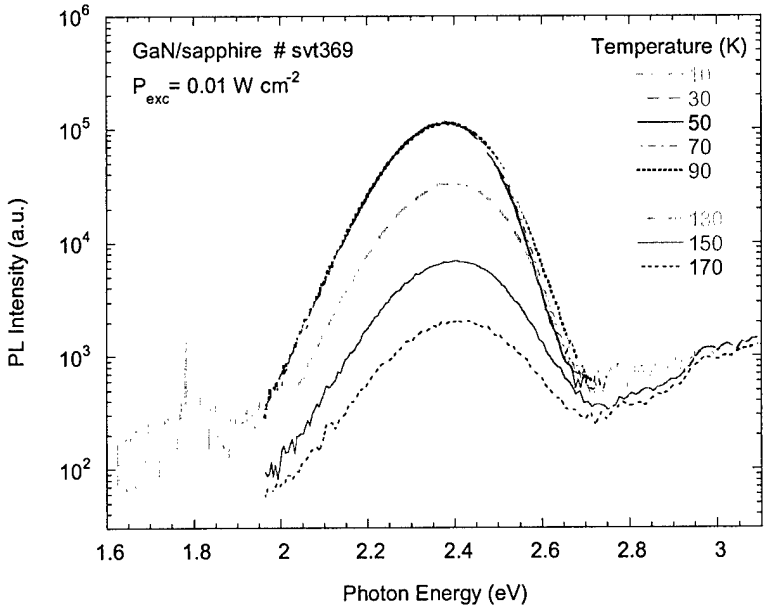

Fig. 7. Variation of the PL spectrum with temperature in the sample with dominating green band.

respectively [2]. Fig. 7 demonstrates transformation of the green PL band with temperature in the sample where this band dominated. One can see that the shape of the band remains nearly unchanged (some broadening will be discussed below) and its maximum slightly shifts to the larger energy side. Position of the band maximum as a function of temperature is shown in Fig. 8. The total blue-shift of the green band in the temperature range 10-200 K is about 30 meV. Note that slightly different positions of the PL band maximum in different samples (Fig.8) can be explained, at least partly, by the interference-related modulation of the spectrum similar to this one seen on Fig. 1.

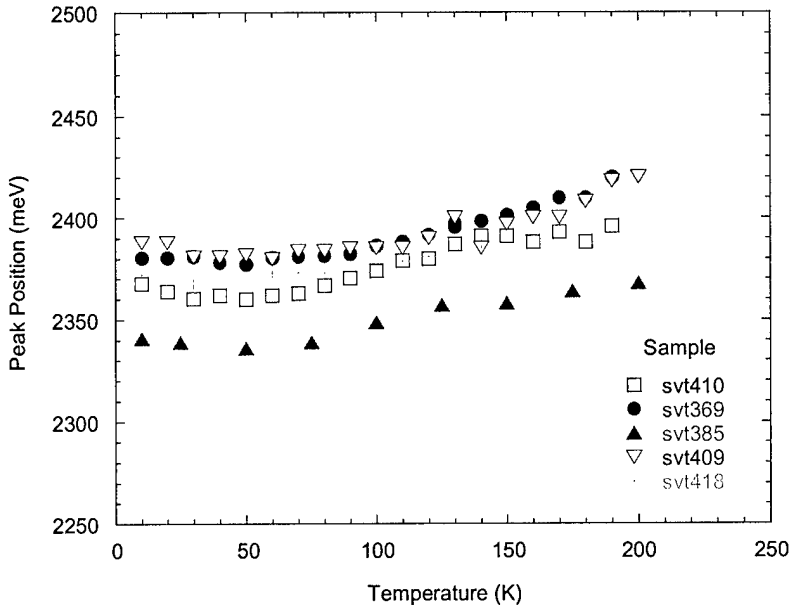

Fig. 8. Position of the green PL band maximum as a function of temperature.

The temperature-induced shift, opposite to the shift which can cause the variation of gap energy (the gap width decreases on about 30 meV in this temperature region), is typical for defects with strong electron-phonon coupling [8]. A similar shift has been observed for the 2.5 and 2.9 eV bands in undoped GaN [2].

The PL spectrum and the temperature-induced behavior of PL for defect with strong electron-phonon interaction can be described in terms of the configuration coordinate (CC) model [3]. Figure 9 shows an example of one-dimensional CC model. The curves 1-3 are adiabatic potentials of the defect representing its total potential energy (electronic and nuclear). The lowest energy potential (curve 1) corresponds to the ground state of the defect (acceptor is totally filled with electrons in n-type GaN). Generation of a hole in the valence band increases the potential energy of the considered system (a defect and a hole) on the energy of the gap width E_g. So, the curve 2 corresponds to the ground state of the defect if the photogenerated hole is taken into account. The photogenerated hole can be captured by the defect and after emission of several phonons the defect will come to the excited state (transition E-F-A). The equilibrium positions of the ground and excited states are displaced from one another and the displacement R_0 is a measure of the electron-phonon coupling. In the simplest case the electronic state interacts with a single localized vibrational mode of frequency ω_0. In many practical

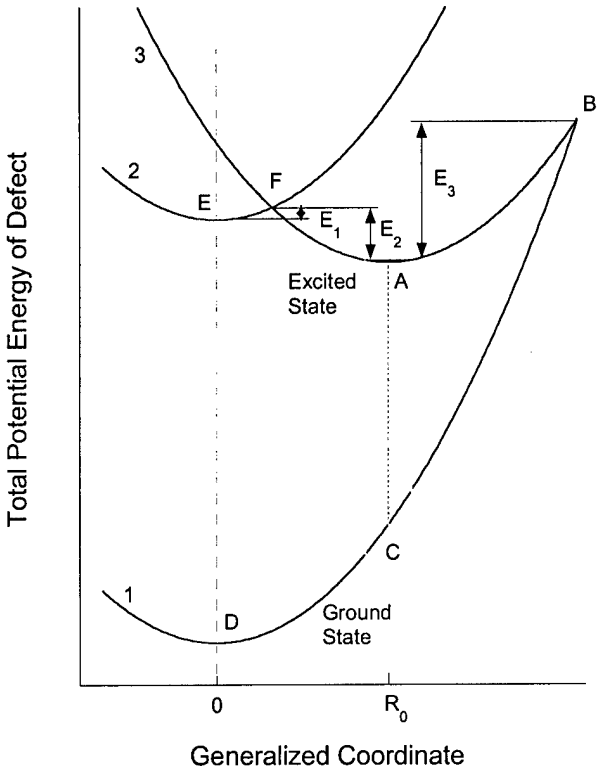

Fig. 9. Configuration coordinate diagram for defect with strong electron-phonon coupling.

cases, the coupling with one of vibrational modes is much stronger than with others, what justifies the one-dimensional approach. The phonon frequencies in the ground and excited states may be different, ω_0^g and ω_0^e, respectively. At low temperatures only the zero vibrational level (with energy of ½ ω_0 from the adiabatic potential minimum) is occupied. Let us consider the recombination process (transition from the curve 3 to the curve 1). The optical transition is much faster than the nuclear motion, hence the transition is vertical (A-C in Fig. 9). The maximum of the PL band will be observed at the photon energy equal to the difference between the adiabatic potentials for the ground and excited states taken at point R_0. Due to the zero-level oscillations of the defect and essential shift of the adiabatic potentials (large value of R_0) the PL band has essential width even at zero temperature. The zero-temperature width of the band is larger when the displacement R_0 is large, when the vibrational frequency of the defect in the excited state is high (the value of ½ ω_0 is large) and the vibrational frequency of the defect in the ground state is high (in this case the ground state parabola is sharper). With increasing the temperature, more and more higher phonon states of the excited state are occupied and the width of PL band increases. The full-width at half maximum (FWHM, or W) of the PL band in the CC model is given by [2]

$$W(T) = W(0)\sqrt{\coth\left(\frac{\hbar\omega_0^e}{2kT}\right)} = \left(\sqrt{8\ln 2}\,\frac{S_{em}\hbar\omega_0^g}{\sqrt{S_{ab}}}\right)\sqrt{\coth\left(\frac{\hbar\omega_0^e}{2kT}\right)}, \qquad (2)$$

where S_{ab} and S_{em} is the Huang-Rhys factor of the defect, respectively in the case of absorption and emission. At high temperatures the band-width is proportional to $T^{1/2}$ and

at low temperatures it is temperature independent. Thus, it is possible to find $W(0)$ and ω_0^e from the temperature dependence of the FWHM of PL band.

Variation of the FWHM of the green band with temperature is shown in Fig. 10 for 3 samples. From the fit of the experimental data by Eq. (2) the energy of the phonons in the excited state, $\omega_0^e = 23$ meV, is found. The parameter $W(0)$ is obtained to vary from 220 to 250 meV for different samples.

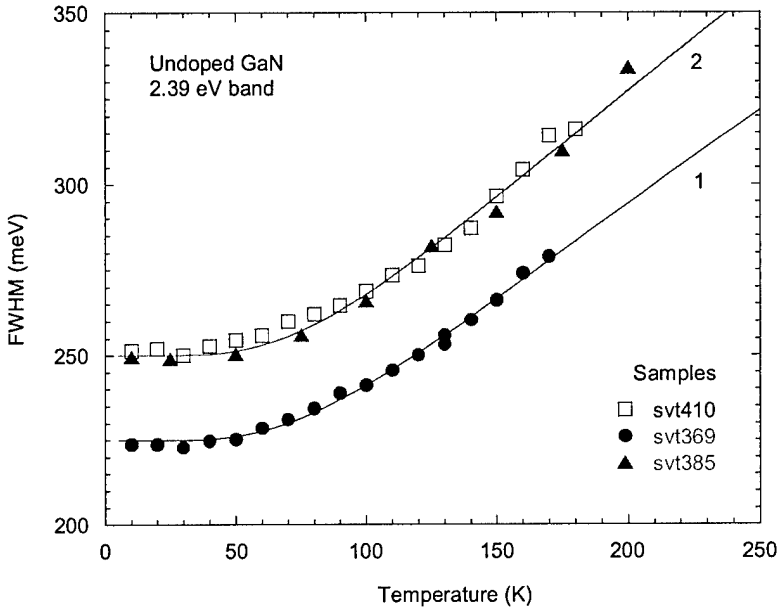

Fig. 10. Temperature dependence of the green band-width. The solid curves are fit by Eq. (2) with the following parameters: W(0) = 220 meV (1); 250 meV (2); $\omega_0^e = 23$ meV (1,2).

The value of ω_0^e calculated for the green band is much smaller than that found previously for three other deep defects in GaN (52 meV for the YL; 40 meV for the 2.5 eV band and 43 meV for the 2.9 eV band) [2]. We believe that this is the frequency of the local vibrational mode of defect (in some cases the coupling with the lattice phonons, for example with LO phonons, dominates). We can roughly estimate the strength of the electron-phonon coupling in assumption that vibrational frequencies in the ground and excited states are the same [3]. Indeed, assuming that $\omega_0^e = \omega_0^g = \omega_0$ and $S_{ab} = S_{em} = S$, it is easy to find from Eq. (2), using $W(0) = 220$-250 meV and $\omega_0 = 23$ meV, that S = 13-17.

As was demonstrated in Ref. 2, the above used simplification can lead to a large discrepancy, if the vibrational frequencies in the ground and excited states are actually different. To find actual values of the vibrational energy and the coupling strength in both the ground and excited states, one should know the energy of the zero-phonon transition E_0 (which is equal to the distance between the minima of the adiabatic potentials for the ground and excited states). We believe that this information can be obtained from the PL excitation spectrum, as it was previously done for the YL in GaN [9]. Nevertheless, even now rough estimates with variation of the value of E_0 in reasonable range show that the Huang-Rhys factor is higher than 10 both for the ground and excited state of the defect

responsible for the green PL band and the vibrational energy in the ground state is close to or less than 23 meV.

Let's turn to the thermal activation energies for the red and green PL bands. The observed value of thermal quenching (about 120-140 meV) is surprisingly small for such deep defects. Two possibilities for the thermal quenching of PL can be considered.

First mechanism comprises escape of nonequilibrium holes from the acceptor to the valence band (transition from point A to point E in diagram of Fig. 9). The activation energy for this process is E_2 (Fig. 9). The released hole can recombine through other channels, thus reducing the PL from the considered type of defects. The quenching of PL from the previously studied deep defects in undoped GaN (responsible for the 2.2, 2.5 and 2.9 eV bands) occurs via this mechanism [1,2]. However, in case of the red and green PL bands, which have smaller thermal and larger optical ionization energy, this mechanism implies much larger displacement of the adiabatic potentials in the ground and excited states of the defect, i.e. much stronger electron-phonon coupling.

Another mechanism of PL quenching comprises nonradiative recombination of the bound hole with a free electron at elevated temperature (transition A-B-D in diagram of Fig. 9). The quenching of PL occurs with activation energy E_3 in this mechanism (Fig. 9). The defects with such quenching mechanism usually have very low radiative efficiency and act as killers of PL [3]. Nonradiative defects in GaN is a stumbling block for development of the high quality optical devices of new generation.

An increase of the red PL band intensity in the range 10-60 K (Fig. 6) can be explained in two ways. First, it can be a barrier for a free hole to be captured by the acceptor (E_1 in fig. 6). With increasing temperature, the increased oscillations of the defect facilitate the capture process. An alternative explanation involves a second, metastable state of the defect. We just touched fundamental problems of deep defects which are important as for understanding of the processes in the material and devices, so for elimination or, on contrary, usage of defects.

The above discussion concerned deep defects revealing themselves through broad PL bands. Besides, some defects reveal themselves through capture and releasing of excitons. Excitons bound to the shallow hydrogen-like defects are well studied, whereas the binding of excitons by deep point defects and by structural defects, abound in GaN, is under future investigations. A set of sharp PL peaks in the range of photon energy 3.0-3.45 eV has been observed in some GaN samples, see Fig. 3. Experiments with variation of the excitation power demonstrate no saturation of PL intensity and no shift of peak position (at least for some of the observed peaks). This is typical behavior for the exciton emission. With increasing temperature from 10 to 150 K the peaks are thermally quenched (Fig. 11). To find the nature of the structural defects, which can bind excitons, we conducted experiments with selective etching. It was established previously that photoelectrochemical (PEC) wet etching in some conditions can leave unetched wires which presumably contain threading dislocations [9]. A tentative PEC wet etching of one of the samples with several sharp peaks in the 3.0-3.45 eV range has culminated in dramatic change of the PL spectrum (Fig. 12). More detail studies are needed.

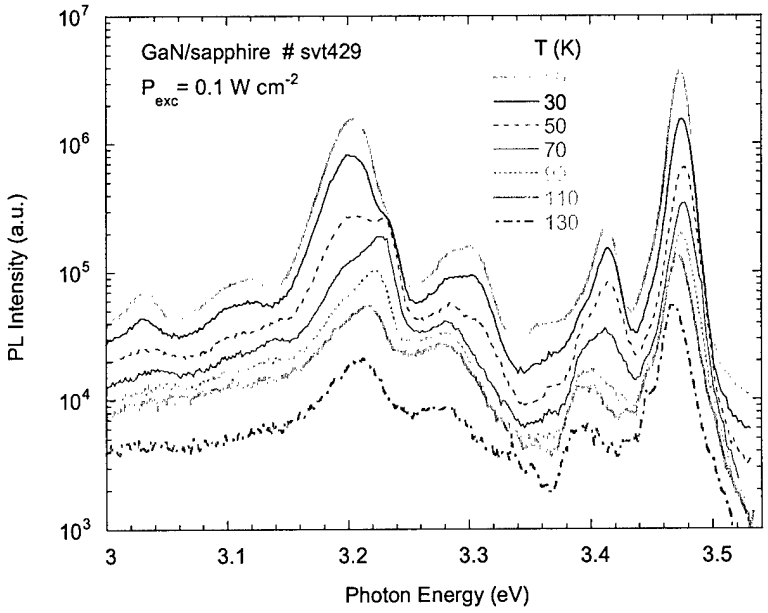

Fig. 11. Temperature induced transformation of PL spectrum from the GaN sample grown in SVT system with RF plasma source of nitrogen.

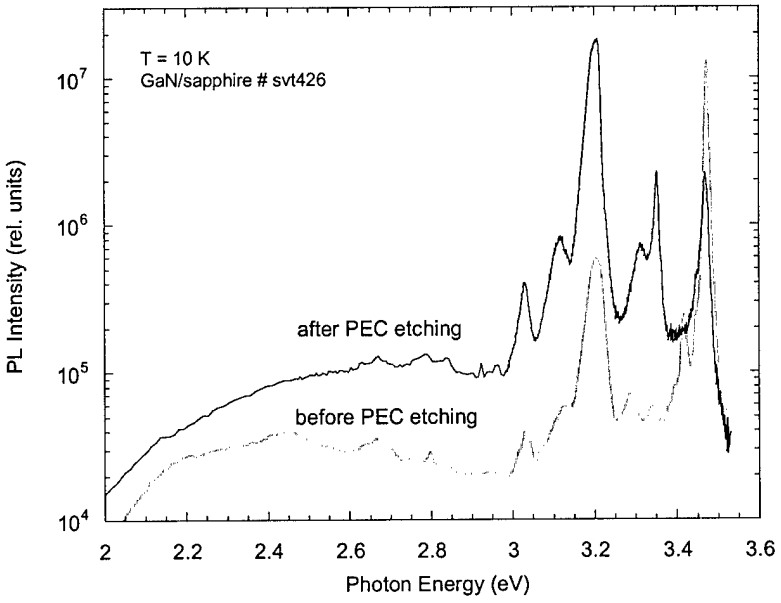

Fig. 12. Effect of PEC wet etching on PL spectrum of the GaN sample.

Problems which can be solved

Defects in GaN, other nitrides and related devices play a key role in future development of high quality optical and electrical devices. Understanding and identification of defects even in undoped GaN is only the first step in the odyssey of GaN based device development. From specific problems which should be solved by our group in the nearest future, the following tasks are related to defect studies.

1. Transient PL experiments. They can confirm suggestions about type of optical transitions and provide information about defect (capture cross-section, concentration).
2. Resonant excitation of defect and measurements of the excitation PL spectra for certain PL bands. This information can reveal the energy of the zero-phonon line, which facilitates constructing the model of defect.
3. ODMR studies can provide unique information about nature and structure of deep defects. We are already collaborating with colleagues from NRL on this topic.
4. Selective and uniform etching experiments can help in defect identification and obtaining its distribution in the grown material.

References

1. M. A. Reshchikov, F. Shahedipour, R. Y. Korotkov, M. P. Ulmer, and B. W. Wessels, JAP **87**, 3351 (2000).
2. M. A. Reshchikov, F. Shahedipour, R. Y. Korotkov, M. P. Ulmer, and B. W. Wessels, Physica B **273-274**, 103 (1999).
3. A. M. Stoneham, "Theory of Defects in Solids", Clarendon Press, Oxford (1975).
4. M. A. Reshchikov, G.-C. Yi, and B. W. Wessels, PRB **59**, 13176 (1999).
5. R. Dingle and M. Ilegems, Sol. St. Comm. **9**, 175 (1971).
6. K. Kornitzer, M. Mayer, M. Mundbrod, K. Thonke, A. Pelzmann, M. Kamp, R. Sauer, Materials Science Forum **258-263**, 1113 (1997) [Trans. Tech. Publications, Switzerland 1997].
7. S. Fischer, G. Steude, D. M. Hofmann, F. Kurth, F. Anders, M. Topf, B. K. Meyer, F. Bertram, M. Schmidt, J. Christen, L. Eckey, J. Holst, A. Hoffmann, B. Mensching, and B. Rauschenbach, J. Cryst. Growth **189-190**, 556 (1998).
8. S. Shinoya, T. Koda, K. Era, and H. Fujiwara, J. Phys. Soc. Japan **19**, 1157 (1964)
9. C. Youtsey, L. T. Romano and I. Adesida, APL **73**, 797 (1998).

Appendix E: PHOTOENHANCED ELECTROCHEMICAL (PEC) ETCHING of GaN

Improvements in the performance of GaN-based devices depend on the quality of epitaxial materials and the development of device processing technologies. In particular, effective etching techniques are essential for forming facets for GaN light emitters (LED and LASER), defining mesas for photodetectors, and gate recessing for HFET devices.

The group III nitrides are distinguished by their unusual chemical stability, a characteristic, which has required unique challenges for device processing. Indeed, the group-III nitrides have high bond energies compared to conventional III-V semiconductors. The high bond strengths and wide bandgaps make them essentially chemically inert and highly resistant to bases or acids at room temperature. Elevating the temperature (>120 °C) in a wet etching process can increase the etch rates but the difficulties to find a effective mask layer make this process not suitable for GaN-based device processing. Therefore, most of processing of III nitrides is currently conducting by dry plasma etching [1-4]. High-density plasma or energetic ion assisted etching were used to get a smooth etch surface and highly anisotropic sidewalls with high etch rates. But there are several disadvantages of dry etching, including the generation of ion-induced damage and difficulty in obtaining smooth etched sidewalls [1]. So there have been a number of efforts examining assisted wet etching techniques. Photoenhanced electro-chemical (PEC) wet etching has been demonstrated for etching of GaN; PEC etching has the advantage of low surface damage and low equipment cost [5-11].

The PEC process utilizes ultraviolet illumination to generate electron-hole pairs at the semiconductor surface, which enhance the oxidation and reduction reactions within an electrochemical cell. Indeed, the basic mechanism for the photoenhanced etching is the oxidative dissociation of the semiconductor into its component elements (thereby consuming the photogenerated holes) and the subsequent reduction of the oxidizing agent in the solution by reaction with the photogenerated electrons. Increasing absorption of incident optical radiation with energy greater than the GaN bandgap energy also increases the supply of holes at the surface, therefore enhancing the etch rates. In most cases, n-type GaN material is readily etched, in contrast to p-type samples where the inability to confine photogenerated holes at the semiconductor-electrolyte interface prevents etching.

Minsky et al [5] first demonstrated room temperature PEC etching of n-GaN using 45% KOH/H_2O (1:3) and HCl/H_2O (1:10) solutions. They utilized HeCd laser to illuminate unintentionally doped n-type GaN samples; so, etch rates of ≈ 400 nm/min and 40nm/min were obtained for the KOH and HCl solutions, respectively. No significant etching was observed in the absence of optical illumination. Lu et al. [6] proposed a photoassisted anodic etching process using Hg lamp illumination and a buffered aqueous solution of tartaric acid and ethylene glycol to get etch rates of 160nm/min in unintentionally doped GaN.

Youtsey et al [7-9] have demonstrated the etching of n-GaN in KOH solutions using a broad-area Hg lamp; the electrochemical cell used in this experiment, included a Pt wire as system cathode and a thin Ti metal film as mask. For a 0.04 molar solution and for light intensities between 10 and 50 mW/cm^2, etch rates were proportional to the light intensity and varied from 50 to 300 nm/min. Highly anisotropic etch profiles were obtained with the rough surfaces. However, under conditions of very low KOH

concentrations (<0.01 M) and high light intensities, anisotropic etch profiles with smooth surfaces were obtained [7]. It was postulated that the following oxidation reaction is responsible for the decomposition of GaN [7]:

$$2GaN + 6h^{+} \rightarrow 2Ga^{3+} + N_2 \uparrow$$

Peng et al [10] used deep UV 253.7nm mercury line source to etch unintentionally doped n-type GaN layers using aqueous phosphorus acid (H_3PO_4) and potassium hydroxide solutions of different pH values.

Also, Stocker et al. [11] presented a two-step method to fabricate wet-etched very smooth InGaN/GaN laser cavities using photoenhanced electrochemical wet etching followed by molten KOH crystallographic etching.

In addition to the etching of GaN required for device fabrication, it has been shown that PEC etching can also reveal dislocations in n-GaN. First, Rotter et al. [12] observed etch pits with hexagonal symmetry with a density in the range $(5\text{-}10)\times10^{9}$ cm^{-2}, corresponding to the dislocation density in the films. Youtsey et al. reported about nanometer-scale "whiskers-like" features obtained by etching n-GaN in 0.02 molar KOH solution with a light intensity of $10mW/cm^2$ [13, 14]. The whiskers had diameters of ≈25nm and lengths of ≈200nm. Moreover, with cross-sectional transmission electron microscope (TEM) image, they demonstrated the propagation of dislocations from the unetched GaN into the whiskers. The reduced etch rates at dislocation sites leading to whisker formation can be explained by a spatially varying concentration of photogenerated holes on the GaN surface.

Weimann et al. [15] have modeled dislocations as negatively charged Coulomb centers; so, these negatively charged centers can become sinks for photogenerated holes thereby locally depressing the concentration of holes that can participate in the etching. Therefore, the lateral selective etching of the crystalline material around the dislocation areas in the n-GaN films takes place.

The characterization of dislocations in nitride films is carried out principally through transmission electron microscopy (TEM), a process which requires extensive sample preparation. With PEC etching, under precise etching conditions, it is possible to reveal the original distribution of dislocations within the nitride film. So, after the etching, with AFM and SEM measurements, it is possible to count the "whisker-like" structures in a fixed area of the image permitting to establish the dislocation density of the material.

We employed the PEC wet etching to reveal the density of dislocations and to study defects in GaN. The GaN samples for these experiments consisted of ≈ 1-2 μm thick unintentionally doped n-type GaN layers ($n \sim 10^{17}\text{-}10^{18}$ cm^{-3}) grown on sapphire substrates by molecular beam epitaxy (MBE). A standard lift-off process was used to obtain a 100 nm Ti metal mask on the periphery of the sample; also, the Ti mask served as a better contact in photocurrent conduction. The Ti contacts were annealed. The PEC etching process of GaN films was carried out in an electrochemical cell consisting of a Teflon sample holder and a Ni-Cr wire cathode. The samples were clipped to a Teflon base using a stainless steel washer and immersed in a not-stirred 0.02 M KOH solution. No bias was applied between the sample and the cathode during the etching. A He-Cd laser (325 nm) was used as a source of the UV radiation. The samples were typically

etched during 1 hour under moderate density of the incident radiation (0.1-1 W/cm^2). An ammeter was used to monitor the photocurrent within the electrochemical cell. The current flow between the sample (anode) and the Ni/Cr cathode is proportional to the reaction rate at the semiconductor/electrolyte interface, and therefore provides an instantaneous measure of the etch rate of the GaN film.

Characterization of the etched samples was carried out using a Tencor alpha-step profilometer to measure the etched depths, while the surface morphology was examined by both scanning electron microscope (SEM), and tapping-mode Digital atomic force microscopy (AFM).

Figure 1 shows variation of the photogenerated current through the electrochemical cell during 1h etching process. The beginning of the illumination corresponds to a rapid increase in current flow, followed by a gradual decrease during the process. The decrease of the current can be attributed to depletion of the photogenerated electron-hole pairs around dislocations during the etching of GaN material.

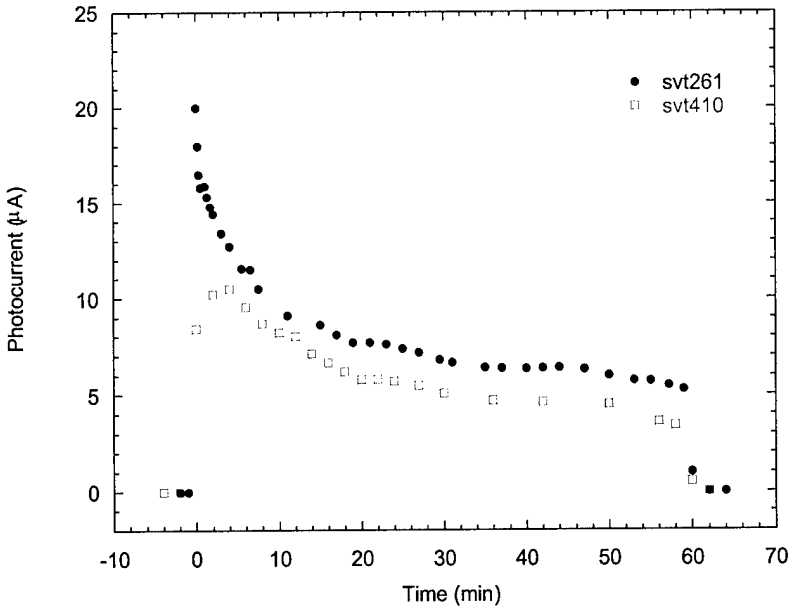

Fig.1 Variation of the photogenerated current during the PEC etching.

For the above-mentioned etching conditions, the etch rate varied from 3 to 20 nm/min. We tentatively attribute the difference in the etch rate to different quality of the GaN samples. No significant etching has been found in the regions not subject to the laser illumination.

The scanning electron microscopy (SEM) images in Fig.2 reveal the "whiskers-like" structures produced by the selective PEC etching process. According to these images, the lateral size of the whiskers is of the order of 100 nm. In assumption that these features replicate the distribution of dislocations [13, 14], we have estimated the density of dislocations in this sample to be 2×10^9 cm^{-2}.

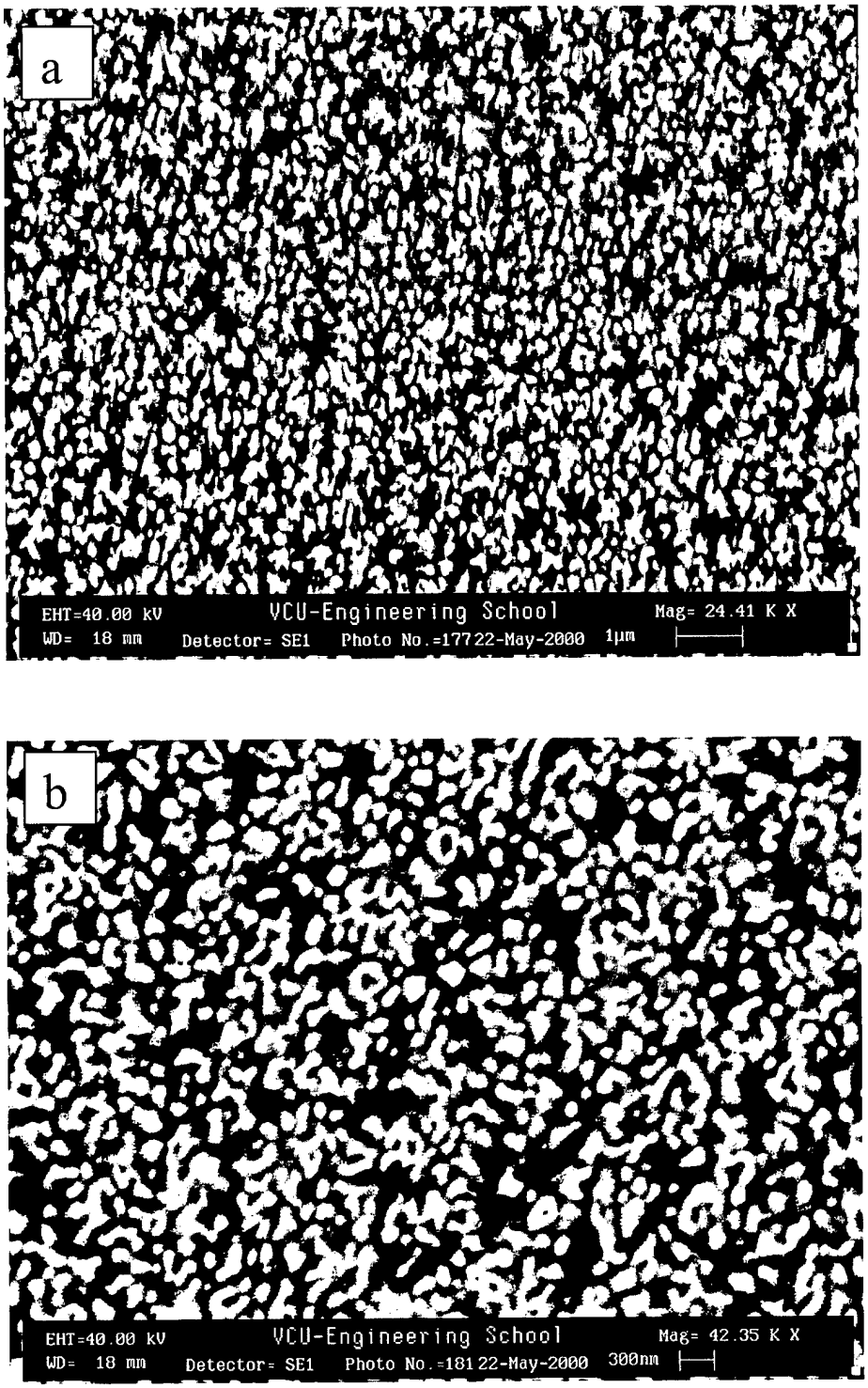

Fig.2 Scanning electron microscopy images of the etched region of GaN sample # SVT 261. (a) Low magnification SEM image (b) High magnification SEM image of the same region; 100nm features are visible on the etched region.

The atomic force microscopy (AFM) of the same etched region is shown in Fig. 3. We have estimated the height of the "whiskers-like" features to be of the order 700 nm and the lateral size about 100 nm from. The density of dislocations estimated from the AFM images is quite close to the value obtained from the SEM study. In the high resolution AFM image (Fig. 3b), we can clearly see the 100 nm-scale free-standing features on the etched surface.

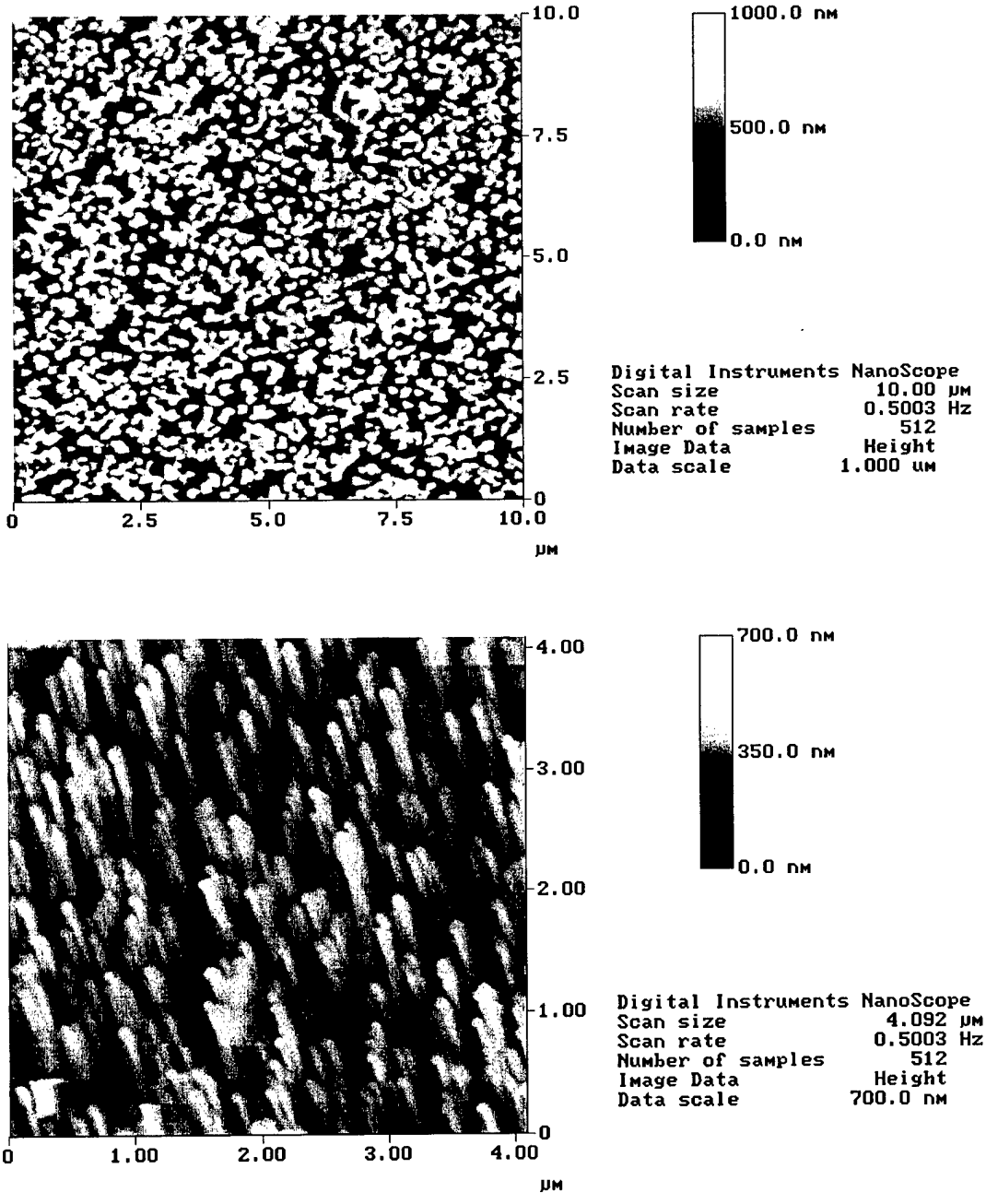

Fig.3 AFM images of PEC etched region of the GaN sample SVT 261.

We performed AFM cross-section measurements in the same etched sample (Fig.4). From this figure, we can see that the selective etching takes place in GaN material producing narrow vertical columns on the surface of sapphire; in this image the height of columns exceeds 1μm.

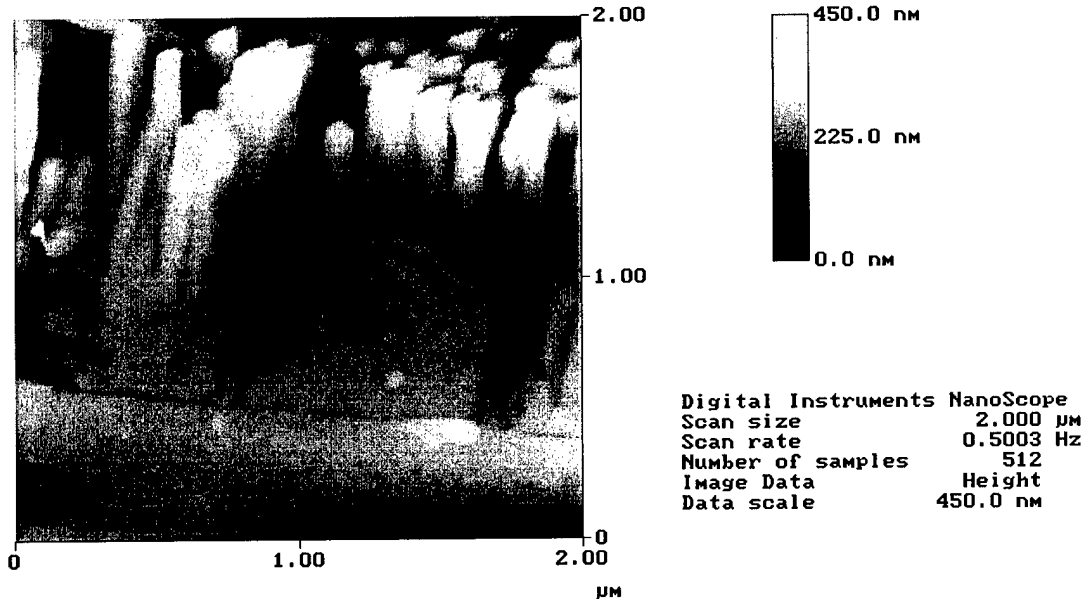

Fig.4 Cross-section AFM image of PEC etched GaN sample SVT 261.

The PEC etching process shows considerable promise and may be used for several device fabrication steps, as well as for the estimation of dislocation densities in n-GaN films.

Photoluminescence study of GaN etched by PEC method

In few recent works, the photoluminescence (PL) was used in characterization of the etched GaN samples [16-18]. Brown et al. [16] observed an increase of PL intensity on about one order of magnitude after the reactive-ion etching with argon plasma. The authors explained this effect by introduction of shallow donors during etching [16]. Hwang et al. [17] reported a relative increase of the yellow luminescence (YL) and shallow donor-acceptor pair (DAP) band in the room PL spectrum after PEC wet etching at high power of Hg-arc lamp, which was used as a UV source for the etching. The authors of Ref. 17 assumed that the gallium vacancy-oxygen complex ($V_{Ga}O_N$) was created by the PEC etching and suggested a questionable mechanism of recombination responsible for the observed PL. Reuter et al [18] observed very small changes of the PL intensity and PL spectrum after PEC wet etching, namely, the DAP PL intensity increased about twice and an exciton peak revealed negligible decrease in intensity along with the blue shift. The blue-shift of the exciton peak and an increase in the DAP PL intensity was explained by the fact after etching a layer closer to the buffer/substrate interface has been studied which exhibits stronger residual strain and higher concentration of impurities [18]. The authors of Ref. 18 also measured the PL from the sample with wires, which can be obtained by PEC etching at particular circumstances [13], and compared it with PL from the same sample after the wires were etched away. They observed that the PL intensity from the sample with wires is about 5 times weaker than from the flat surface after removal the wires. Besides, not essential variation in the PL spectrum has been observed: the YL intensity increased and DAP PL intensity decreased about 2 times relatively the exciton peak. The authors explained the observed decrease of PL in the wires region by predominance of the nonradiative recombination in wires, which presumably contain dislocations [18].

It should be noted that the study of defects from the etched GaN samples by PL method just started. One should be careful in comparing the absolute values of the PL intensity between different samples because PL set-ups are very sensitive to optical alignment and it is easy to get difference of PL intensity two times just due to improper alignment. Another problem is that whereas defects can be introduced by etching itself, there may be different distribution of defects in the depth of the GaN layer (note that PL gives information about thin, about 100 nm surface layer due to high absorption of the exciting light).

Experimental results

We have conducted first experiments with PL from the etched GaN. The same conditions of PEC etching were used, whereas the etch rate varied much from sample to sample. In most of the studied samples the wires with high density have been observed by AFM method. PL from the PEC etched and unetched regions of the samples were compared. Different excitation density (in the range 10^{-3}-100 W/cm^2) of the continuous wave He-Cd laser was exploited. Most of experiments have been carried out at 10 K.

The preliminary analysis of the experimental results reveals high complexity of the studied problem. Let us consider the effect of PEC etching (conducted at the same conditions) on three different samples. A sample H958 was grown by HVPE method in Lincoln laboratories, samples svt261 and svt426 were grown by MBE method with

ammonia as nitrogen source. All three samples exhibited vertical wires after etching, yet of different density and shape.

The effect of PEC etching on the HVPE grown sample is shown in Fig. 5.

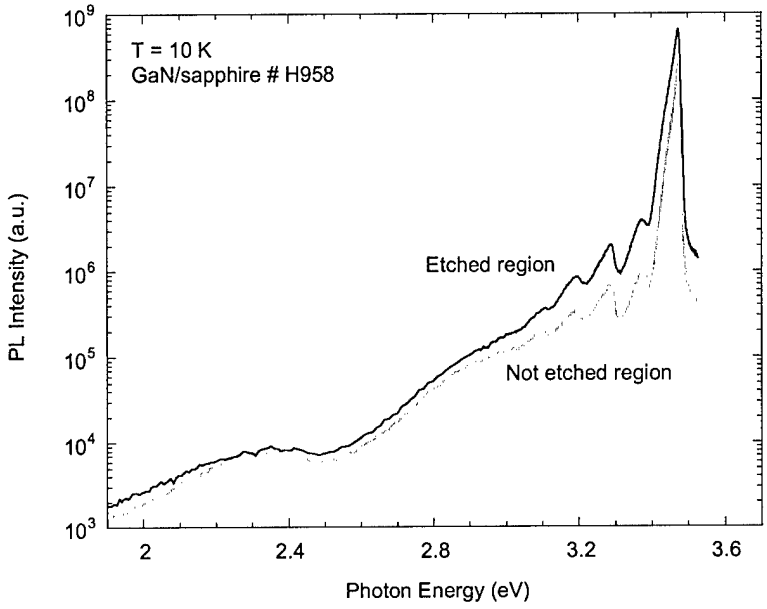

Fig. 5. Effect of PEC wet etching on the PL spectra of the HVPE grown sample. Position of the exciton peak maximum, 3.4735 eV, is the same in etched and unetched regions. Quantum efficiency increased from 7 to 18 % after PEC etching. Exciton emission comprises 98% of the radiative recombination.

In contrast to expected and observed in Ref. 18 decrease of PL intensity from the etched region rich with vertical wires, our sample exhibits strong increase of radiative recombination. The quantum efficiency of radiative recombination increased from 7 to 18 % after PEC etching. About 98 % of the radiative efficiency fall on the exciton emission. The shape of the spectrum, which involved exciton emission, DAP related peaks and two broad bands – blue and yellow, remained nearly the same. The PEC etching caused an increase in intensity of about 1.5-3 times for all PL bands, the same result has been obtained in wide range of excitation density (from 10^{-3} to 1 W/cm^2). The observed phenomenon can be explained by reduction of nonradiative defects in the etched region. The fact that intensities of all PL bands increased approximately in equal degree confirms this conclusion. This is very surprising result considering that dislocations are expected to act as nonradiative defects. Note also that the absolute value of the radiative efficiency in the exciton range is extremely high, which suggests very low concentration of nonradiative defects. One can assume that dislocations (at least the type of them present in the studied sample) are not the most efficient killers of the optical yield in GaN. It is known that point defects with very strong electron-phonon coupling can be efficient centers of nonradiative recombination. Possibly the region etched by selective PEC method contains higher concentration of such nonradiative defects in this sample.

Preliminary experiments showed that different samples exhibit different effect of PEC etching on PL properties of the material. A comparison between the low-

temperature PL from the etched and not etched areas of two other samples, grown by MBE method, demonstrates striking difference (Figs. 6 and 7).

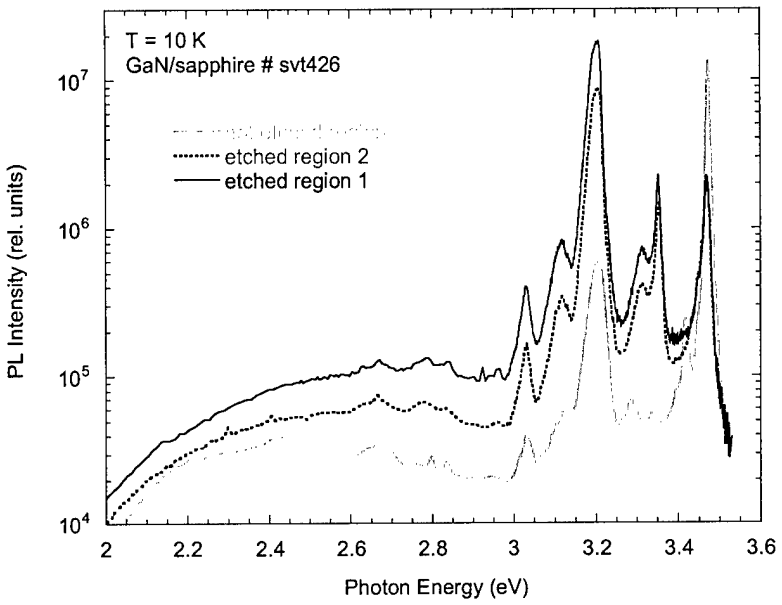

Fig. 6. PL spectra from the reference region and from two points of the PEC etched region in the MBE grown sample. Integrated PL intensity from the exciton bound to shallow donor (peak at 3.474 eV), dominating in the reference sample, decreased 3 times after etching.

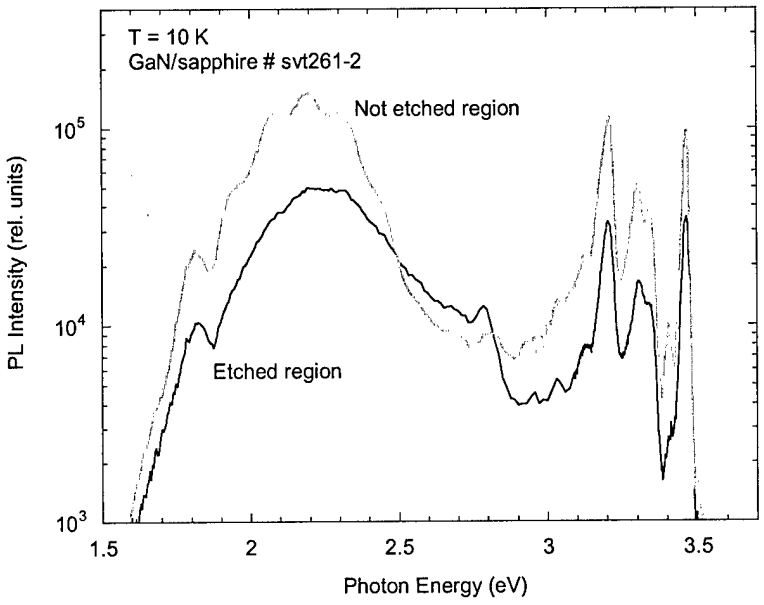

Fig. 7. PL spectrum from the MBE grown GaN sample in the etched and reference region. Maximum of the exciton peak is at 3.466 eV in both cases. Long-range oscillations with a period of about 115 meV observed better in the 2-2.5 eV range are due to interference of PL between the surface and interface of GaN layer.

In one of the samples an increase of the integrated PL intensity and an emergence of new sharp peaks at the photon energy of about 3.3-3.35 eV takes place after PEC etching (Fig. 6). An intensity of the 3.474 eV line, which is attributed to the exciton bound to a shallow donor, decreases. With increasing excitation density up to 100 W/cm^2, the sharp peaks in the photon energy region 3.0-3.5 eV do not shift and their intensity does not saturate. Such behavior is typical for excitonic emission. We assign tentatively the sharp PL peaks in the range 3.0-3.4 eV to excitons bound to different structural defects in this sample. In another sample PL intensity decreased in more or less the same degree for all PL bands after PEC etching (Fig. 7). To draw the conclusion, we need to carry out experiments at different samples and to compare the PL results with the results of other studies. It is important also to compare the effect of selective etching (when the vertical wires are formed) with the flat etching to estimate the possible role of non-uniform distribution of defects in the thickness of GaN layer.

References:

1. S. J. Pearton, J. C. Zolper, R. J. Shul, F. Ren, J. Appl. Phys. **86**, 1 (1999).
2. R. J. Shul, S. P. Kilcoyne, M. Hagerott Crawford, J. E. Parmeter, C. B. Vartuli, C. R. Abernathy, and S. J. Pearton, Appl. Phys. Lett. **66**, 1761 (1995).
3. B. Molnar, C. R. Eddy, Jr., and K. Doverspike, J. Appl. Phys. **76**, 6132 (1995).
4. C. B. Vartuli, J. D. MacKenzie, J. W. Lee, C. R. Abernathy, S. J. Pearton, R. J. Shul, and Appl. Phys. Lett. **66**, 1761 (1995).
5. M. S. Misky, M. White, and E. L. Hu, Appl. Phys. Lett., **68**, 1531 (1996).
6. H. Lu, Z. Wu, and I. Bhat, J. Electrochem. Soc. **144**, L8 (1997).
7. C. Youtsey, I. Adesida, and G. Bulman, Appl. Phys. Lett., **71**, 2151 (1997).
8. C. Youtsey, I. Adesida, L. T. Romano, and G. Bulman, Appl. Phys. Lett., **72**, 560 (1998).
9. I. Adesida, C. Youtsey, A. T. Ping, F. Khan, L. T. Romano, and G. Bulman, MRS Internet J. Nitride Semicond. Res. 4S1, G1.4 (1999).
10. L.-H. Peng, C.-W. Chuang, J.-K. Ho, C.-N. Huang, and C.-Y. Chen, Appl. Phys. Lett., **72**, 939 (1998).
11. D. A. Stocker, E. F. Schubert, K. S. Boutros, and J. M. Redwing, MRS Internet J. Nitride Semicond. Res. 4S1, G7.5 (1999).
12. T. Rotter, D. Uffmann, J. Ackermann, J. Aderhold, J. Stemmer, and J. Graul, Mat. Res. Soc. Symp. Proc. **482**, 1003 (1998).
13. C. Youtsey, L. T. Romano, and I. Adesida, Appl. Phys. Lett., **73**, 797 (1998).
14. C. Youtsey, L. T. Romano, R. J. Molnar, and I. Adesida, Appl. Phys. Lett., **74**, 3537 (1999).
15. N. G. Weimann, L. F. Eastman, D. Doppalapudi, H. M. Ng, and T. D. Moustakas, J. Appl. Phys. **83**, 3656 (1998).
16. S. A. Brown, R. J. Reeves, C. S. Haase, R. Cheung, C. Kirchner, and M. Kamp, Appl. Phys. Lett. **75**, 3285 (1999).
17. J. M. Hwang, J. T. Hsieh, H. L. Hwang, and W. H. Hung, MRS Internet J. Nitride Semicond. Res. **5S1**, F99W11.73 (2000).
18. E. E. Reuter, C. Youtsey, I. Adesida, and S. G. Bishop, Mat. Res. Soc. Symp. Proc. **482**, 997 (1998).

Appendix F

EFM and Cross Sectional AFM Electrostatic Force Microscopy

Recently, it has been demonstrated that electrostatic force microscopy (EFM) is able to map the domain structure of ferroelectric crystals with 50 nm lateral resolution.[1-3] A much higher lateral resolution of 4-5 nm has been reported on silver nanocrystals.[*R. M. Nyffenegger, R. M. Penner, and R. Schierle, Appl. Phys. Lett. 71, 1878(1997)*] In comparison with other techniques, EFM is nondestructive and has the advantage that the magnitude and distribution of the electric field in the vicinity of the sample surface can be imaged. EFM data are collected (in our lab) using a Digital Instruments Nanoscope IIIa controller and a MultiMode scanning probe microscope operating in tapping mode.

EFM can be performed in two ways: by detecting the electric field gradient and by detecting the surface potential. In both cases surface topography is first taken by tapping mode AFM. Then the cantilever will ascend to a certain height away from the surface, and follow the stored surface topography at the lift height above the sample, while responding to electric influences on the second scan.

1. *Electric field gradient imaging*: Albeit non-quantitative, electric field gradients imaging can provide interesting insight into the nature of both defects and piezoelectric effect in nitride semiconductors.[*P. M. Bridger, Z. Z. Bandic, E. C. Piquette, and T. C. McGill, Appl. Phys. Lett. 74, 3522(1999)*] To detect the electric field gradient, a voltage is applied to a metallic coated AFM tip that is scanned across the surface at a constant tip-sample separation. The force on the tip is expressed by: $F=(q_s q_t)/(4\pi\varepsilon_0 z^2)+1/2(dC/dz)(V_{applied}-V_{contact})^2$, where (dC/dz) is the vertical derivative of the tip-sample capacitance, and $V_{contact}=\phi_m-\chi_{GaN}-\Delta E_{fn}-\Delta\phi$ is the contact potential between the tip metallization and GaN semiconductor. In the formula, ϕ_m is metal work function, χ_{GaN}=4.2eV is the electron affinity of GaN, $\Delta\phi$ is band bending caused by surface states, and ΔE_{fn} is the Fermi level position in the GaN referenced to the bottom of the conduction band. Phase differences induced by electrostatic forces on the oscillating tip are detected and give a qualitative measurement of local electric field gradients. This type of imaging favors samples with smooth surface but large contrast in electric force gradient due to material difference or regions at substantially different potentials.
2. *Surface Potential Imaging*: Surface potentiometry can quantitatively map the change in surface potentials due to charge redistribution. To detect the local surface potential, an oscillating voltage is applied directly to the AFM tip; $V_{applied}=V_0\cos(\omega t)$. The tip feels a force of $F=(dC/dz)(V_{tip}-V_{sample})V_{applied}$. In order to determine the surface potential of the sample, the tip voltage is adjusted by a feedback loop to equal the sample potential so that the tip feels no force. A preferred sample for surface potential imaging is one with rough surface topography or smaller potential variations.

Cross Sectional—XAFM and XEFM

Despite the great success of cross-sectional STM in the study of III-V heterostructures, it is still difficult and time consuming in sample cleaving, probe tip preparation, and UHV operation. In contrast, operation of AFM is considerably easier for routine characterization. There has been report on XAFM for III-V.[*A. J. Howard, O. Blum, H. Chui, A. G. Baca, and H. Crawford, Appl. Phys. Lett. 68, 3353(1996)*]

We developed, on our Digital Instrument Nanoscope IIIa AFM system, cross-sectional AFM technique that allows us to probe nitride properties which are representative not only of the surface, but also of the underlying layers. It can provide a wealth of information including interface roughness, point and extended defects, nucleation conditions and buffer layer growth, strain inhomogeneities[*Huajie Chen, R. M. Feenstra, R. S. Goldman, C. Silfvenius and G. Landgren, Appl. Phys. Lett. 72, 1727(1998)*] in MQW and QD sturctures, etc.

To perform XAFM, one has to load the cut sample onto a special cross-section holder. One should be very careful to align the cantilever onto the right position of the sample cross-section, by the aid of a mono-piece eye lens. Tapping mode is normally used to have better image. The image will better reflect the cross-section after fast Fourier transform (FFT) or other image processing.

Similar to regular EFM, we can also perform EFM on cross-sectional samples. The presence of inversion domains from the starting point of growth could be traced by XEFM. Strain-induced piezoelectric fields in different layers could be analyzed. Spontaneous polarization, which has comparable contribution to charge density at heterointerface, will be identified by mapping the electric field or potential as well.

What we have done by EFM and XAFM

EFM

1. Electric field gradient image was shown in Fig. 1. Electrostatic forces were measured as a function of tip voltage to rule out topographical artifacts. Variation in the induced surface charges result in a force differential between the tip and the surface that increases with tip voltage, which can be observed in a series of EFM images as shown in Fig. 1. It is a MBE grown GaN sample which starts with low temperature nitridation and low temperature AlN buffer layer. In fig 1, we can see that when V_{tip} is zero, there is almost no variation of EFM image beside the residual background, though the surface topography in the same area has a lot of troughs and islands. With increasing V_{tip}, the variation of electrostatic force becomes more and more clear, with most induced charges concentrated at the boundaries of the islands, thus making EFM image more or less resemble the pattern of topography.

Fig. 1 EFM image of SVT397, left side is tapping mode AFM image of the same region. (a) voltage on tip is zero; (b) voltage on tip is 5V.

XAFM

Fig. 2 (a) Cross-sectional AFM image of #261 (as-grown, GaN, 1.77um thickness).The bright and amorphous top at the outer surface is a thin layer of metal coating. The image on the left (b) is a high pass fast Fourier transform (FFT).

What we expect from EFM and XEFM

1. Qualitative analysis of electric field distribution with respect to surface topography and/or inversion domains—electric field gradient imaging.
2. Demonstration of the presence of surface states and estimation of surface states density in both Ga- or N-polarity films, by analyzing the barrier energy as a function of the metal work function and semiconductor electron affinity. This could be realized by a series of EFM experiments with different metal-coated tips to change the metal semiconductor work function.
3. Study of the nature of the measured surface charges to understand the roles of charges induced by different defect structures, piezoelectric induced charges, and spontaneous polarization induced charges. The behavior of charge screening effect will also be considered.
4. Comprehensive understanding of the impact of strain (thus piezoelectric electric field), spontaneous polarization, epilayer polarity, on the interface charges and band structure of 2DEG, hence on the device performance of MODFET.[*H. Morkoc, R. Cingolani, and B. Gil, Solid-State Electronics, 43, 1909(1999)*] This could be done by a combined characterization of EFM with both electric field gradient imaging and surface potential imaging, in the hope that each factor affecting the formation of interface charges could be identified and treated semi-quantitatively. For example, dislocation density could be measured by photoelectric chemical etching and characterized by AFM and XAFM; spontaneous polarization induced field could be extracted by separation of the second harmonic EFM signal[*K. Franke, H. Huelz, and M. Weihnacht, Surface Science 415, 178(1998)*] from the base signal. With cross-sectional EFM, the origin of the factors resulting in electric field distribution could be traced, and the screening effect of interface charges could be more cleared out.
5. Investigation of how other basic factors, such as illumination, external strain[*P. M. Bridger, Z. Z. Bandic, E. C. Piquette, and T. C. McGill, J. Vac. Sci. Technol. B17, 1750(1999)*] and variation in defects, could affect the EFM image of nitride semiconductors, to further our knowledge of the fundamental physics as well as polarization engineering.
6. Recent work has shown that chemical etching can selectively etch Ga and N faces of GaN growth.[*M. Seelmann-Eggebert, J. L. Weyher, H. Obloh, H. Zimmermann, A. Rar, and S. Porowski, Appl. Phys. Lett. 71, 2635(1997)*] By combining this technique with AFM, XAFM, EFM, and XEFM it may be possible to control the formation of inversion domains and other defect structures.

References:

1. F. Saurenbach and B.D. Terris, Appl. Phys. Lett. 56, 1703(1990)
2. R. Luthi, H. Haefke, K.-P. Meyer, E. Meyer, L. Howald, and H.-J. Guntherodt, J. Appl. Phys. 74, 7461(1993)
3. T. Hidaka, T. Maruyama, M. Saitoh, N. Mikoshiba, M. Shimizu, T. Shiosaki, L. A. Wills, R. Hiskes, S. A. Dicarolis, and J. Amano, Appl. Phys. Lett. 68, 2358(1996)
4. ....as listed in the text.